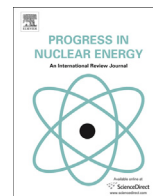




Contents lists available at ScienceDirect

Progress in Nuclear Energy

journal homepage: www.elsevier.com/locate/pnucene

Physico-chemical properties of Chernobyl lava and their destruction products



Andrey A. Shiryaev^{a, b, c, *}, Irina E. Vlasova^b, Boris E. Burakov^d, Boris I. Ogorodnikov^e,
Vasily O. Yapaskurt^f, Alexey A. Averin^a, Alexey V. Pakhnevich^g, Yan V. Zubavichus^h

^a Institute of Physical Chemistry and Electrochemistry RAS, Leninsky pr., 31 korp. 4, Moscow 119071, Russia

^b Department of Chemistry, Lomonosov Moscow State University, Leninskie Gory 1 bld. 3, Moscow 119991, Russia

^c Institute of Ore Geology, Petrography, Mineralogy and Geochemistry RAS, Staromonetny per, 35, Moscow 119017, Russia

^d V.G. Khlopin Radium Institute, 2nd Murinsky av. 28, St.Petersburg 194021, Russia

^e Karpov Physical Chemistry Institute, Vorontsovo Pole str. 10, Moscow 105064, Russia

^f Department of Geology, Moscow State University, Moscow 119991, Russia

^g Paleontological Institute RAS, Profsoyuznaya str. 123, Moscow 117997, Russia

^h NRC "Kurchatov Institute", Akademika Kurchatova Sq. 1, Moscow 123098, Russia

ARTICLE INFO

Article history:

Received 24 January 2016

Received in revised form

28 June 2016

Accepted 1 July 2016

Keywords:

Glass

Ceramics

Nuclear accident

Chernobyl

Corium

Zircon

ABSTRACT

The paper commemorates 30th anniversary of severe nuclear accident at the 4th Unit of Chernobyl NPP. Results of the investigation of radioactive glassy lava-like materials formed as a result of the accident at their current state are presented. Complementary analytical methods: vibrational spectroscopy, XAFS, SEM, EBSD, X-ray tomography, provide new information about structure of the Chernobyl lava matrix and inclusions. Most of these techniques are applied to the lava samples for the first time and allow to derive consistent model of the lava and to resolve some of existing controversies. The glassy matrix of the lava is an anhydrous depolymerised metaluminous glass with signs of devitrification. Principal inclusions are (U,Zr)O_{2-x} and (Zr,U)O_{2-x} solid solutions with tetragonal and monoclinic structures, UO₂ and U-rich zircon. Cracks around large inclusions are observed; some of them could be caused by volume expansion during tetragonal to monoclinic transition in zirconia. The lava accumulations are characterized by different stability against spontaneous destruction, with the pumice-like lava being the least stable, generating radioactive aerosols and particles with sizes up to 250 μm.

© 2016 Elsevier Ltd. All rights reserved.

1. Introduction

The accident at the 4th Unit of Chernobyl Nuclear Power Plant (ChNPP) on 26 April 1986 led to destruction of the reactor core and release of an enormous amount of solid and gaseous radioactive products to the environment due to explosion and subsequent fire. Independent approaches based on ¹³⁷Cs and ⁹⁰Sr fractionation and structural peculiarities of dispersed fuel and corium particles showed that transient (few seconds or less) temperatures immediately prior to the explosion event reached at least 2200–2600 °C leading to reactions between the UO₂ fuel and zircaloy cladding (Burakov et al., 1997a, 2003; Kashparov et al., 1996; Kashparov et al., 1997). The explosion epicenter was presumably localized in

a relatively small volume of the reactor core (Abagyan et al., 1991; Adamov et al., 1988; Kashparov et al., 1997). Though the estimates vary, the amount of fuel dispersed to dust (both inside and outside the reactor building) and expelled from the reactor shaft is estimated as ~4–6% from the total amount of 190 metric tons of uranium (Arutyunyan et al., 2010; Information ..., 1986; Lebedev et al., 1992).

In the RBMK reactors the reactor basement plate is a cylinder 14.5 m in diameter and 2 m in height, filled with serpentinite with bottom and top steel lids interconnected by stiffening ribs and water tubes. During the explosion a 100–110° sector of the basement plate was pushed approx. 4 m down, merging the reactor shaft with a former sub-reactor room 305/2 (e.g., Arutyunyan et al., 2010). The amount of nuclear fuel in the room 305/2 is estimated at 65–80 tons of UO₂ (Borovoi et al., 1998). Before and shortly after the explosion the fuel reacted with zircaloy and later with construction materials (sand, concrete, serpentinite, steel), leading to the

* Corresponding author. Institute of Physical Chemistry and Electrochemistry RAS, Leninsky pr., 31 korp. 4, Moscow 119071, Russia.

E-mail address: shiryaev@phych.ea.ru (A.A. Shiryaev).

formation of so-called lava-like fuel-containing materials (LFCM) or Chernobyl “lava” (Burakov et al., 1994, 1997a,b; Ushakov et al., 1997). Several days after the accident considerable fraction of the initial lava pool spread into other rooms of the reactor building (Burakov et al., 1997a), forming vertical and horizontal flows which solidified into a highly radioactive glassy material with inclusions of high-uranium zircon crystals ($Zr_{1-x}U_x$)SiO₄, particles of molten stainless steel, uranium oxide dendrites and grains, and particles of Zr-U-O phases (solid solutions in the system of UO₂-ZrO₂). Several varieties of the lava are known (e.g., Anderson et al., 1993; Borovoi et al., 1990, 1991a, 1991b; Burakov et al., 1994, 1997a,b; Pazukhin, 1994; Pazukhin et al., 2006; Savonenkov et al., 1991; Trotabas et al., 1993): 1) brown lava, 2) black lava, and 3) much less abundant and less studied polychromatic lava. On the lower levels of the reactor building the flow of brown lava entered water in the bubbler tank forming pumice-like material (Borovoi et al., 1991a; Trotabas et al., 1993). Controversy still exists about the total amount of uranium in all “lava” streams in comparison with initial fuel inventory. Estimates vary from 9–13% (Kiselev and Checherov, 2001) to >80% (Arutyunyan et al., 2010) of total amount of the ChNPP fuel; the rest is believed to remain in inaccessible premises of the reactor, possibly as fuel rods fragments.

Although the microstructure and other properties of the Chernobyl “lava” were extensively studied in the past, in particular, in 1990–1997 (Anderson et al., 1993; Arutyunyan et al., 2010; Borovoi et al., 1990, 1991a, 1991b; Burakov et al., 1994, 1997a,b; Pazukhin, 1994; Pazukhin et al., 2006; Savonenkov et al., 1991; Trotabas et al., 1993), some important features relevant for prediction of their long-term behavior remains poorly studied. The main obstacle is high radioactivity of the samples. We report here new results on present (as of 2014–2015) state of lava samples and aerosols collected inside the “Shelter” building, complementing our recent investigation of radioactivity distribution in the lava samples (Vlasova et al., 2015). Most of the analytical techniques employed by us are applied to the lava samples for the first time and obtained results are important to derive consistent model of the lava and to resolve some of existing controversies.

2. Samples and methods

All samples described in the paper were collected inside the confinement building “Shelter” of ChNPP.

2.1. Bulk lava samples

Bulk lava samples were manually detached under harsh conditions in 1990 by MrVladimir Zirilin of the V.G. Khlopin Radium Institute (St. Petersburg, Russia) from two different types of lava. Small samples described in the current paper represent pieces of much larger specimens (several tens cm³): the fragments of black lava (Sample I, approx. 3 × 1.5 × 1.5 mm in size, Fig. 1A, B, and Sample II ca. 4.5 × 2 × 2 mm in size, Fig. 1C, D) were collected from the lava stream “Elephant foot”, level +6.0 m (Borovoi et al., 1991a; Burakov et al., 1997a); and the fragment of brown lava (Sample III, 3 × 2 mm, Fig. 1E, F) was collected from the steam-discharge corridor at level +6.0 m (Borovoi et al., 1991b; Pazukhin et al., 2003). The fragments were mounted in 1991 into acrylic resin and manually polished in a glove box. For the polishing SiC powder with grain sizes (decreasing during the process) 28/14, 10/5 and 3/1 μm were used; final polishing was performed on dense paper with diamond paste (1/0). After the polishing the samples were stored at laboratory till 2015. This process provided mirror-like finish with virtual absence of a damaged layer as confirmed by successful EBSD analyses of steel droplets (see below). Despite pronounced radiation damage of the resin at the contact with the

lava after 24 years of storage, the surface of LFCM remains mirror-like.

2.2. Aerosol particles

Aerosol particles were collected in 2010–2014 at the distance of 20–30 cm from the lava heap in room 012/7 (level 0.0 m, the first floor of the Bubbler tank (Borovoi et al., 1991a)) using a pack of three Petryanov filters with different particulate retention sizes mounted on the nose of the air blower H810 RadeCo operating for 2 h at a pump rate 100 dm³/min. Daily variations of the air temperature in this room are negligible, annual variations are within 4°C (+9°C in winter and +13°C in summer). Chemical and radionuclide (e.g., ¹³⁷Cs/²⁴¹Am) composition of the particles collected is consistent with composition of the heap (Pazukhin et al., 2003; Ogorodnikov et al., 2013).

2.3. Spontaneously detached individual sub-millimeter particles

These chips were collected in 2013–2014 on the planar cuvette placed for 6 months on the floor 0.50 m in front of a lava heap in room 012/7 (see chapter 2.2). These particles are of particular interest, since their detachment from the lava accumulation appears to be spontaneous. The particular lava agglomeration is mechanically heterogeneous: the internal part is highly porous (pumice-like or granulated, see Fig. 1G, H) since it was formed when hot brown lava stream entered in contact with water in the Bubbler tank, whereas the outer shell is glassy due to rapid quenching (Borovoi et al., 1991a; Pazukhin et al., 2003). The glassy shell was partly broken by researchers. The exact origin of the studied particles – the heaps’ shell or interior or even destruction of eventual pieces of pumice observed in this room – is unclear.

2.4. Experimental details

Several analytical methods revealing different chemical and structural features of the samples were employed. Note that spectroscopic data for the “lavas” were not available before. Quantitative SEM-EDX analyses of the polished samples (described in chapter 2.1) was performed using JEOL JSM-6480LV equipped by Oxford X-Maxⁿ 50 spectrometer and Oxford Nordlys Max2 EBSD detector. Analytical conditions were as following: 30 nm carbon coating, accelerating voltage – 20 kV, electron beam current – 10 nA, working distance – 10 mm. Quantification of detected elements was achieved using the following reference materials: albite, FeS₂, Ca₃Si₃O₉, TiO₂, Cr₂O₃, Mn, Zr, UO₂, and Di-117733, Hbl-143965, Hyp-746, Kfs-143966, Hyp-746 from (Corrections, 1980). XPP-correction was applied. The data are given in mass% to facilitate comparison with literature data, which were mostly obtained using Emission analysis. Semi-quantitative SEM-EDX investigation of loose unpolished aerosol and sub-mm particles (described in chapters 2.2 and 2.3) study was performed using JEOL JSM-6380 LA with JED 2300 analyser. Raman spectra in quasi-backscattering geometry were acquired with Senterra (Bruker) spectrometer with an Olympus BX-51 microscope with long working distance objectives. Excitation wavelengths of 532 and 785 nm were employed. The laser power was kept sufficiently low to prevent sample modification; the spot size was 2–5 μm depending on magnification used. IR reflectance spectra were acquired using SpectrumOne FTIR spectrometer with AutoImage microscope (Perkin Elmer). To assess homogeneity mapping of the whole sample with a 100 μm aperture was performed. In addition, spectra of representative points and of selected inclusions were acquired with up to 256 scans with spectral resolution of 4 cm⁻¹. X-ray microtomography (X-ray micro-CT) of aerosol filters and of

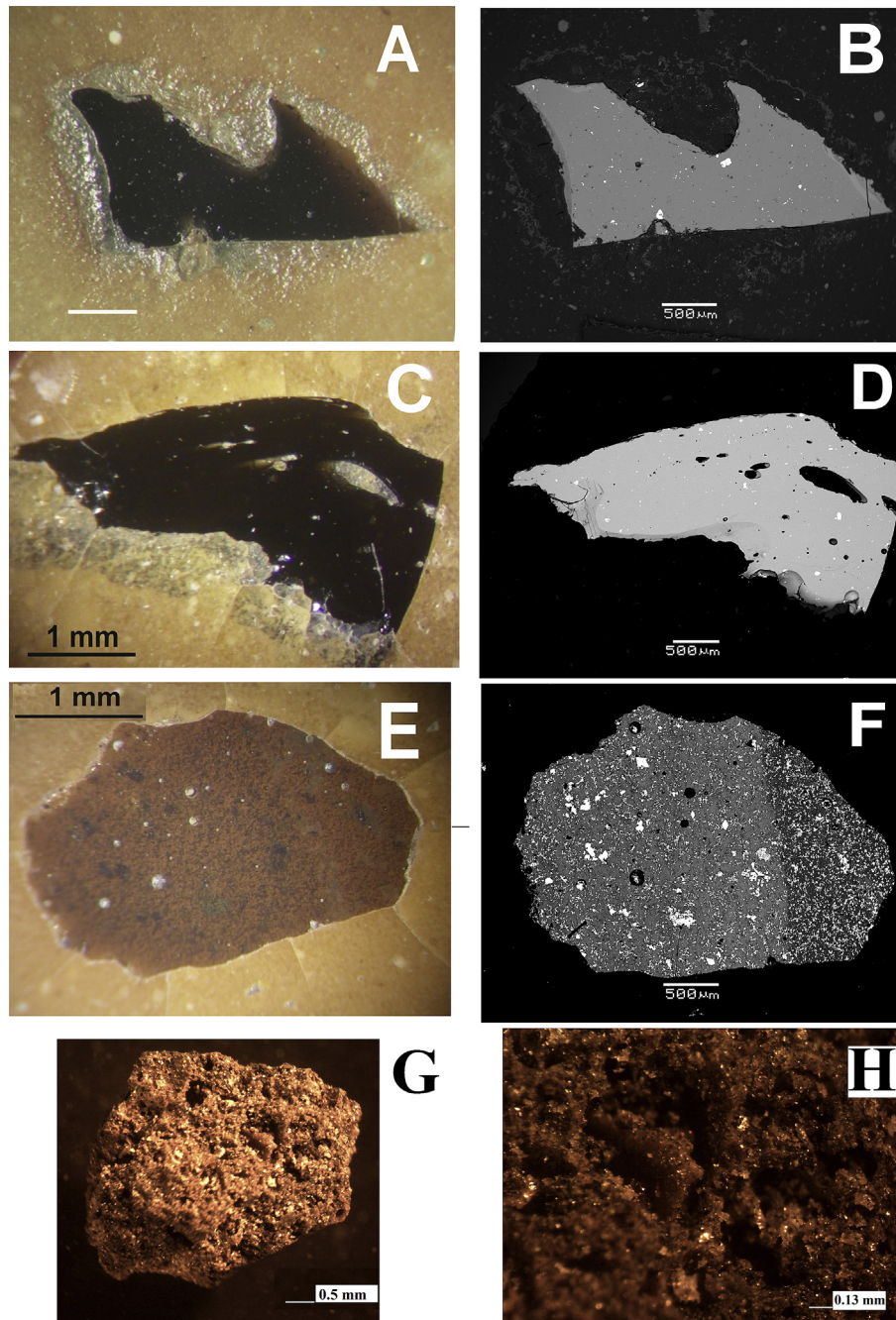


Fig. 1. Optical and SEM images of Chernobyl lava samples. A–D – black lava (Samples I and II), E, F – brown lava (Sample III); G, H – granulated brown lava from room 012/7 (see text). A, C, E, G, H – optical photographs; B, D, F – BSE mode. Note significant radiation damage in surrounding acrylic resin.

detached particles (chapters 2.2. and 2.3) was performed using SkyScan 1172 device. Depending on the sample size and task (aerosol filter or dense glass particle) the tube operating conditions were 29 or 49 kV, beam current 100 μA ; image pixel size was between 1.02 and 11.44 μm . Rotation step – 0.25 deg., frame averaging – 8, random movement – 10, rotation – 180°. The slices were generated using NRecon version 1.6.41. Extended X-Ray Absorption Fine Structure (EXAFS) spectra of U and Zr for the Sample I were acquired at Synchrotron center at Kurchatov Institute (Moscow) in fluorescence mode (Chernyshov et al., 2009).

3. Results

3.1. The bulk samples: texture and chemical composition

SEM images of samples are shown in Fig. 1 and EDX composition data are presented in Tables 1 and 2. The samples consist of glassy matrix with abundant inclusions and numerous gas bubbles of very different size. In some cases the bubbles are in contact with inclusions, but in general they are independent from each other.

Remarkably, the sample of brown lava consists of two chemically distinct parts clearly observable in BSE mode (Figs. 1F and 2A). The main difference between them is the number density of

Table 1

Composition (mass %) of black lava from the Room 217/2, +6.0 m (see paragraph 2.1 and Fig. 1 for details).

Element, mass%	Detection limit (2σ)	Glass matrix of black lava				Inclusions in black ceramics				Bulk black lava from Ref. 3	
		The Sample I (13)	Glass around zircons (7)	Sample II (21)	<i>Ref.1</i>	<i>Ref. 2</i>	Zircon in the sample I (7)	Zircon in the sample II (3)	ZrO ₂ in the sample I (1)		UO ₂ in the sample I (9)
Na	0.06	1.27 ± 0.05	1.11 ± 0.06	1.20 ± 0.07	<i>0.4</i>						4.0 ± 1.4
Mg	0.04	1.64 ± 0.02	1.65 ± 0.02	1.63 ± 0.04	<i>1.2</i>	<i>1.3</i>					3.0 ± 0.4
Al	0.06	4.65 ± 0.03	4.69 ± 0.06	4.56 ± 0.05	<i>2.7</i>	<i>3.8</i>					4.0 ± 0.7
Si	0.12	30.40 ± 0.11	30.52 ± 0.38	30.33 ± 0.35	<i>36.9</i>		14.42 ± 0.30	14.42 ± 0.25			28 ± 4
S	0.04	0.08 ± 0.01	0.09 ± 0.01	0.08 ± 0.02							
K	0.06	1.90 ± 0.03	1.88 ± 0.05	1.87 ± 0.06	<i>1.4</i>	<i>2.7</i>					
Ca	0.08	6.64 ± 0.04	6.67 ± 0.14	6.62 ± 0.23	<i>5.1</i>	<i>8.4</i>					4.5 ± 1.9
Ti	0.04	0.16 ± 0.02	0.16 ± 0.02	0.16 ± 0.02							0.11 ± 0.04
Cr	0.04	0.09 ± 0.02	0.10 ± 0.02	0.10 ± 0.02							0.25 ± 0.08
Mn	0.06	0.19 ± 0.02	0.19 ± 0.01	0.19 ± 0.02							0.32 ± 0.10
Fe	0.06	0.36 ± 0.02	0.36 ± 0.02	0.36 ± 0.12		<i>0.3</i>					0.6–8.5
Zr	0.14	3.08 ± 0.04	2.60 ± 0.51	2.98 ± 0.08	<i>3.3</i>	<i>3.7</i>	46.21 ± 2.13	44.70 ± 2.33	65.36	2.25 ± 0.33	4.0 ± 1.2
Nb	0.14							1.23 ± 0.07			
U	0.16	3.54 ± 0.07	3.23 ± 0.31	3.64 ± 0.13	<i>4.0</i>	<i>3.2</i>	5.16 ± 3.12	6.17 ± 3.48	9.45	85.73 ± 0.60	5.7 ± 1.6
O*		45.31 ± 0.46	45.26 ± 0.49	45.16 ± 0.18			33.33 ± 0.67	33.48 ± 0.68	24.35	12.40 ± 11.32	
Totals		99.17 ± 0.19	98.27 ± 0.97	98.81 ± 0.54			99.11 ± 0.36	100.06 ± 0.12	99.40	99.89 ± 0.56	

* – Oxygen calculated from stoichiometry. Number of analyses is in brackets. Literature data are *in italic*. References: 1 – Pazukhin 1994; 2 – Trotabas et al., 1993; 3 – Pazukhin et al., 2003. Detection limits are the same as in Table 1.

Table 2

Composition (mass %) of brown lava from the Room 210/7 (steam-discharge corridor); +6.0 m (see paragraph 2.1 and Fig. 1 for details).

Element, mass%	Glass matrix of brown lava			Inclusions in brown lava, sample III			BULK brown lava from room 210/7 (18) Ref. [1]
	Sample III, brown lava; "dark" zone (5)	Sample III, brown lava; "grey" zone (5)	<i>Ref. [1]</i>	<i>Ref. [1]</i>	Zircon crystals (3)	Zr-U-O (3)	
Na	1.05 ± 0.02	1.02 ± 0.02		<i>0.5</i>			4.0 ± 0.4
Mg	5.46 ± 0.03	5.21 ± 0.04	<i>3.5</i>	<i>4.3</i>			4.2 ± 1.0
Al	4.43 ± 0.01	4.33 ± 0.03	<i>2.8</i>	<i>4.1</i>			3.6 ± 0.8
Si	29.71 ± 0.04	28.71 ± 0.04		<i>36.5</i>	15.98 ± 0.03		30 ± 5
S	0.04 ± 0.01	0.03 ± 0.01					
K	1.58 ± 0.04	1.52 ± 0.02	<i>1.2</i>	<i>2.4</i>			
Ca	5.96 ± 0.02	5.92 ± 0.05	<i>4.9</i>	<i>7.1</i>			4.8 ± 1.1
Ti	0.15 ± 0.02	0.18 ± 0.01					0.15 ± 0.05
Cr	0.21 ± 0.02	0.24 ± 0.02					0.27 ± 0.09
Mn	0.42 ± 0.01	0.45 ± 0.03					0.41 ± 0.14
Fe	0.17 ± 0.03	0.23 ± 0.04		<i>0.2</i>			0.89 ± 0.20
Zr	2.36 ± 0.05	3.35 ± 0.10	<i>2.7</i>	<i>2.7</i>	40.89 ± 1.28	60.40 ± 1.66	3.71 ± 0.60
U	1.92 ± 0.05	3.21 ± 0.12	<i>2.4</i>	<i>1.9</i>	11.26 ± 3.12	16.18 ± 4.36	83.72 ± 1.68
O*	46.32 ± 0.02	45.44 ± 0.02			31.74 ± 1.15	23.42 ± 0.46	12.56 ± 0.62
Totals	100.79 ± 0.27	100.33 ± 0.20			99.87 ± 0.43	99.14 ± 1.20	100.72 ± 0.57

* – Oxygen calculated from stoichiometry. Number of analyses is in brackets. Literature data are *in italic*. References: 1 – Burakov et al., 1997b; 2 – Pazukhin, 1994.

microinclusions and in composition of the glass matrix (Table 2). The glass matrix of the darker inclusion-rich part is poorer in U (2.2 vs. 3.6 wt% UO₂ in the brighter glass) and Zr (3.2 wt% vs. 4.5 wt% ZrO₂) with slightly higher content of MgO and Al₂O₃. The transition between the two parts is smooth. It appears that the darker part also contains brighter domains and numerous signs of rapid glass crystallization (pyroxene dendrites, see below). Detailed examination of the images (Fig. 2A) shows that the brighter part is rather patchy and contains many diffuse darker spots. The darker domains are often anisometric with orientation roughly parallel to the contact of the dark and bright parts. Presumably, these domains represent boundary layers surrounding precipitates. Their elongation reflects gradual glass solidification during slow motion of the cooling lava flow.

The most obvious explanation of the heterogeneity studied sample lies in high viscosity of the lava flows. Most studied lava flows possess layered structure, though the bulk composition of various layers is fairly constant (Pazukhin et al., 2002a). The layered structure is explained by the fact that the sampling localities are

relatively distant (up to 50 m) from their common source (presumably room 305/2) and high viscosity of the flow easily leads to stratification due to arrival of several portions of the lava. Variations in the number density of the inclusions and related differences in chemical composition of the glassy matrix are likely related to variations in the quench rates. Presumably, the darker part was quenched at a much higher rate than the grayish part leading to formation of numerous urania dendrites. Flow patterns formed during solidification are clearly seen in some of the samples, see Fig. 2B.

It is interesting to note that chemical composition of both studied types of the lava (black and brown) remains fairly constant in direction from bulk to surface or to a bubble (apparent minor variations in total sum of the elements are within measurement error). This indicates that diffusion of volatile elements such as Na was not very significant on the last stages of the lava flow motion when the temperature approached glass transition temperatures (approx. 800–850 °C (Gonchar and Zhidkov, 2002)).

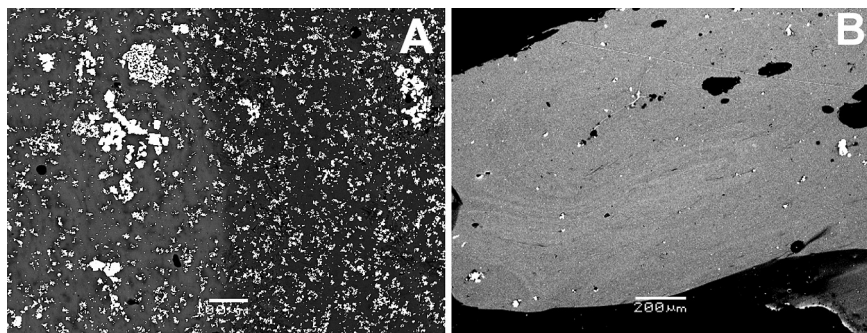


Fig. 2. BSE images. A – Brown lava (sample III), anisotropy of dark inclusions and heterogeneity of the darker part are observed. B – black lava (Sample II), flow pattern is visible.

3.2. Structure of the glassy matrix

Unpolarised Raman spectra recorded with excitation wavelength of 532 nm for several spots on both types of the lava samples show features typical for metaluminous glass (Fig. 3A) (Mysen and Toplis, 2007). The ratio of principal Q^n units is $Q^2 > Q^3 > Q^1$, which suggests that Q^2 are the principal depolymerised structural units in the lava (McMillan, 1984). Depolymerised nature of the glassy matrix is supported by Infra-red reflectance spectra, see Fig. 3B. The main reflectance peak is observed at $1084\text{--}1088\text{ cm}^{-1}$, which is markedly lower than in vitreous silica (1150 cm^{-1}) due to decreased Si-O-Si bond angle following from network modification by cations (Sweet and White, 1969). Intensity of low-frequency part of Raman spectra is comparable to the high-frequency region ($800\text{--}1200\text{ cm}^{-1}$), with the most prominent bands at 340, 460, 480 and a shoulder at 580 cm^{-1} . This region is difficult to interpret unambiguously in glasses of complex chemical composition. A weak peak at $800\text{--}805\text{ cm}^{-1}$ might correspond to a very small amount of $\text{Fe}^{3+}\text{-O}$ bonds, being in line with generally highly reducing state of the lava. However, this peak was also observed in Fe-free metaluminous glasses (Mysen and Toplis, 2007) and in our case assignment of this peak to iron seems to be less relevant.

Importantly, the lava matrix is anhydrous as suggested both by IR mapping and numerous Raman spectra recorded both with 532 and 785 nm excitations. The OH-groups are encountered only in inclusions-rich zones (see Fig. 3B and below). This is not surprising since experimental modeling of the lava formation (Krasnorutskyy et al., 2010, 2012) showed that minimal temperature of their synthesis cannot be less than $1450\text{ }^\circ\text{C}$. Based on concentrations of ^{125}Sb on the walls of room 304/3 adjacent to the inferred lava source it was suggested that temperature of the lava was at least $1500\text{ }^\circ\text{C}$

(Borovoi et al., 1999). Limited wettability of the lava (contact angles for water $60\text{--}68^\circ$ (Zhidkov et al., 2000)) also does not favor incorporation of noticeable amounts of moisture.

Speciation of uranium and zirconium in black lava Sample I was assessed by X-ray Absorption spectroscopy (XAFS). The beam $\sim 0.5 \times 0.2\text{ mm}$ in size was aimed at center of the specimen, but exact position cannot be indicated. XAFS spectrum of U at L_{III} -edge (Fig. 4A, B) shows absence of “uranyl” shoulder, indicating that uranium is present as U(IV). Fourier transform of the spectrum is typical for U-containing glasses (e.g., Stefanovsky et al., 2009). The second coordination sphere (U-U scattering path) due to UO_{2+x} is weakly pronounced, indicating small fraction of uranium in precipitates or highly disordered crystalline lattice of urania inclusions. The latter explanation is in odds with Raman scattering from large ($>10\text{ }\mu\text{m}$) UO_2 inclusions and with results of powder and single crystal X-ray diffraction which indicates high crystalline quality of the urania inclusions (see below). As discussed in (Vlasova et al., 2015) apparent discrepancy of XAFS/SEM and autoradiography might be explained by fortuitous selection of the volume sampled by XAFS or by differences in crystalline perfection (and stoichiometry?) of small and large UO_2 inclusions. Note that investigation of powdered sample of LFCM from steam-discharge corridor and of the pumice-like material using X-ray photoelectron spectroscopy (presence of U-containing inclusions can not be excluded) also showed dominance of reduced forms of uranium – U^{3+} and U^{4+} (Teterin et al., 1994).

XAFS spectra of Zr K-edge show that the Zr environment in the Sample I differs from that in crystalline and metamict zircon (Fig. 4C, D) but is similar to Zr dissolved in silicate glass (Farges and Rossano, 2000). In silicate glasses 6-coordinated Zr promotes polymerization of the silicate network by forming Zr-Si-O bonds.

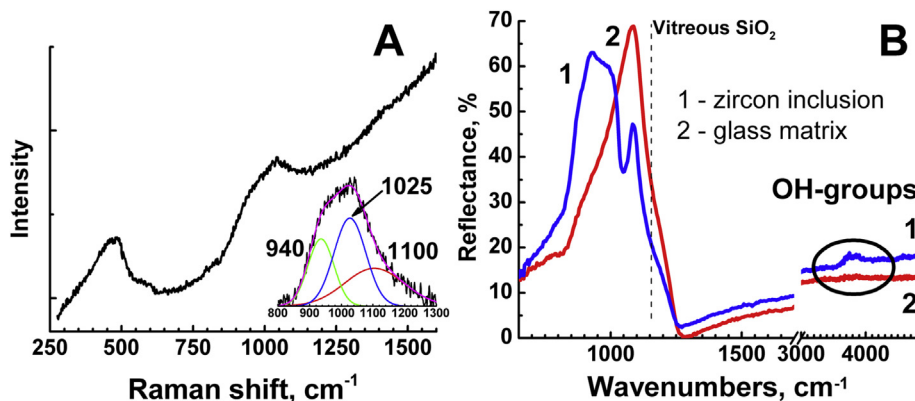


Fig. 3. Representative raman (A) and IR reflectance spectra (B) of the glassy matrix and of region surrounding zircon inclusion. Inset in A shows decomposition of part of the Raman spectrum into contributions from Q^n units (see text). Vertical line in B shows the reflectance peak position in pure vitreous SiO_2 (1150 cm^{-1}). Note break of the abscissa on B.

3.3. Inclusions

In line with previous studies of Chernobyl lava (e.g., Anderson et al., 1993; Burakov et al., 1997a; Troabas et al., 1993), we have observed inclusions of several phases: 1) UO_{2+x} with Zr admixture, 2) ZrO_2 with U admixture and Zr-U-O phases with variable Zr/U ratio, 3) high-uranium zircon (“chernobylite”), $(\text{Zr}_{1-x}\text{U}_x)\text{SiO}_4$, 4) silicate (pyroxene) dendrites due to devitrification of the glassy matrix. Whereas phases of zirconia-uranium solid solutions are known to occur during interaction between zircalloy and UO_2 in experiments as well as under conditions of severe nuclear accident at Three-Mile Island NPP in 1979 (Hofmann et al., 1989; Bottomley and Coquerelle, 1989; Brown et al., 1989), formation of high-uranium fully crystalline zircon is a unique feature of the Chernobyl accident.

3.3.1. Urania

Inclusions of urania are represented by dendrites, rounded inclusions and by relatively large pieces (up to $\sim 50\text{--}70\ \mu\text{m}$). In most cases the urania contains a Zr admixture, indicating formation in overheated fuel rods (e.g., Burakov et al., 1997a). Notable exception is the largest piece of UO_2 in our specimen of brown lava, most of which is Zr-free: only few subgrains in contact with $(\text{Zr}_{1-x}\text{U}_x)\text{SiO}_4$ crystal (Fig. 5A) contain small admixture of Zr. Such heterogeneity of Zr distribution qualitatively resembles some of ChNPP hot particles (Anderson et al., 1992a; Burakov et al., 1994, 1997a,b). This inclusion likely represents fragment of an undissolved fuel pellet. Note that undestroyed pieces of fuel rods and core fragments were observed in brown lava samples from room 304/3, immediately adjacent to the proposed common lava “birth place” – room 305/2. At least some of these undissolved fuel pieces are characterized by low burn-up degree and corresponding lower heat generation (Borovoi et al., 1998).

Raman spectra of all studied urania inclusions – dendrites, rounded blobs and even inclusions in zircon crystals are similar (Fig. 5B). The spectra are dominated by strong asymmetric peak at

$1165\ \text{cm}^{-1}$ with a shoulder at $\sim 1150\ \text{cm}^{-1}$ due to crystal electric field transition. According to (Manara and Renker, 2003) the presence of this peak indicates only small deviations of UO_{2+x} from ideal stoichiometry ($x < 0.7$). Peak at $452\ \text{cm}^{-1}$ is due to U-O stretch in UO_2 , the band at $590\ \text{cm}^{-1}$ probably corresponds to damaged urania (Graves, 1990).

3.3.2. Zirconia and Zr-U-O phase

Other important and abundant phases are uranium-bearing zirconia and Zr-U-O (Fig. 6). The mean composition of the studied Zr-U-O grains is approx. 60 mass% Zr and 16 mass% U (Table 2). This phase most likely serves as a substrate/precursor for growth of U-rich zircon (e.g. Burakov et al., 1997a; see below). Its structure is still not known in detail, but XRD investigation of individual inclusions extracted from lava fragments by partial dissolution in HF shows presence of amorphous fraction and crystalline zirconia-like monoclinic and tetragonal phases (Burakov, 2013a).

Electron-backscatter diffraction (EBSD) and Raman spectra of the Zr-U-O inclusions confirm presence of tetragonal ZrO_2 phase (Fig. 6 B, C). Raman spectra of different Zr-U-O grains reveal mixture of two series of bands with variable relative intensity. Besides peaks of monoclinic ZrO_2 ($171, 184, 374\ \text{cm}^{-1}$) present in all of the studied Zr-U-O grains, five peaks at $140, 254, 469, 603$ and $623\ \text{cm}^{-1}$ due to the Raman-active modes of tetragonal ZrO_2 phase (Kim et al., 1993; Kim and Hamaguchi, 1997) are also observed. Therefore, three independent methods – X-ray and electron diffraction and Raman spectroscopy show that the Zr-U-O inclusions in the brown lava contain zirconia of two different crystalline structures: monoclinic and tetragonal. The presence of the tetragonal phase is explained by extensive doping of zirconia by uranium, since it has been demonstrated (Voronov et al., 1958; Wolten, 1958) that an admixture of UO_2 may stabilize high-temperature ZrO_2 modifications. The Zr-U-O phase most likely represents altered eutectic melt formed before the explosion as a result of UO_2 -zircalloy interaction at high temperature (Burakov et al., 1997a). It is important to mention that the high-temperature zirconia modifications may spontaneously

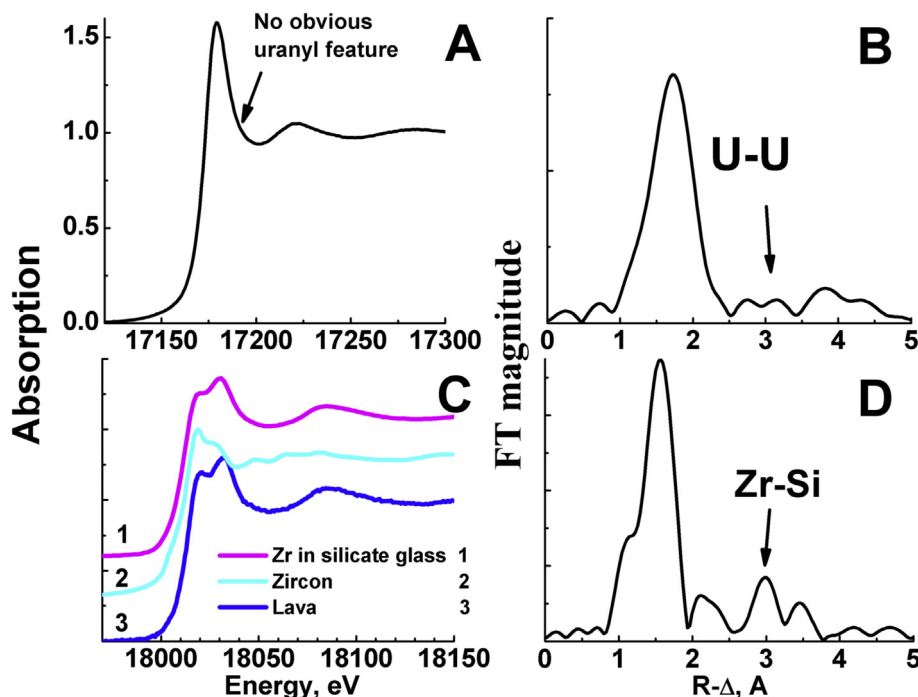


Fig. 4. X-ray absorption spectra (left side) and their Fourier transforms (right side) for U LIII-edge (A, B) and Zr K-edge (C, D) for the black lava sample I.

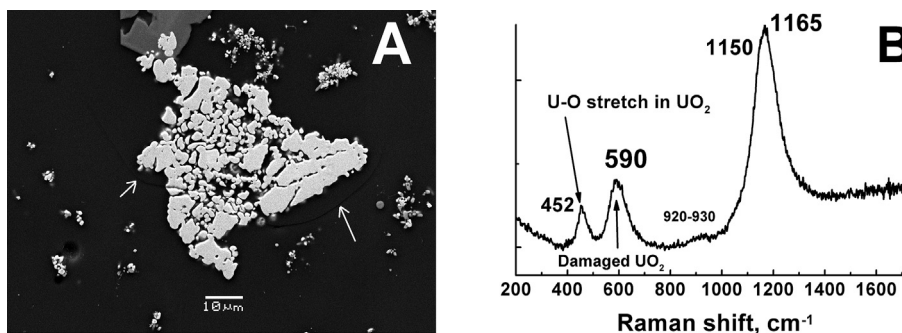


Fig. 5. A – Large inclusion of UO_2 , probably undissolved fuel pellet. Note crack development around the inclusion. Arrows point to crack developed around the inclusion. B – Raman spectrum of UO_2 inclusion.

convert to monoclinic phase during interaction with moisture (Chevalier and Gremillard, 2009). This transformation is accompanied by significant volume expansion. In lava this reaction may lead to cracking and destruction. The phase transformation may also be induced by self-irradiation from uranium, since vacancies and cations charge play decisive role for relative stability of zirconia phases (Chevalier and Gremillard, 2009). Extensive cracks around the Zr-U-O inclusion on Fig. 6 might indicate occurrence of the transformation, although micro-Raman investigation does not show direct correlation between the ZrO_2 phase and cracks.

3.3.3. High-uranium zircon ($\text{Zr}_{1-x}\text{U}_x\text{SiO}_4$ (“chernobylite”))

Images of typical zircon inclusions are shown on Fig. 7. Uranium content varies significantly even in individual crystals. The mean value of U concentration in zircon from the brown lava is higher than in zircon from the black lava (11.3 vs 5.6 wt%). The concentration of U in high-uranium zircon from Chernobyl lava reach 15 wt%, which is in line with previous results (e.g. Burakov et al., 1997a; Geisler et al., 2005; Trotabas et al., 1993). Such concentrations of uranium exceed what has been measured in synthetic samples obtained so far and are extremely rare for natural metamict zircon (e.g., Shalaeva et al., 2015; Zamyatin et al., 2013., and refs. therein). Detailed Raman investigation (Geisler et al., 2005) has shown that uranium in “chernobylite” does form solid solution. Fig. 7B shows Raman spectra of zoned “chernobylite” crystal (black lava Sample I) acquired in central, intermediate and peripheral zones and X-ray map of U distribution as revealed by EDX analysis (Fig. 7A, inset). Using data from (Geisler et al., 2005) we estimate that UO_2 concentration in the analyses spots are ~4, 6, 4 wt%, correspondingly; these values correlate with the EDX results (with allowance to limited positioning precision). In every point zircon remains crystalline with no signs of amorphisation. Remarkably,

both IR reflection (Fig. 3B) and Raman (Fig. 7B) spectra from this crystal show presence of OH-groups.

Some zircon crystals observed in this work possess perfect morphology, the others are still (partly) attached to parent Zr-U-O phase (see below) and many demonstrate cracks filled with surrounding glass and features of skeletal morphology (Fig. 7A, C, D). These morphological peculiarities probably indicate very uneven growth process with large variations in supersaturation. The majority of the crystals show pronounced growth zoning with variations in U-content. Most likely, the “chernobylite” inclusions have crystallized in a common source of the lava, some of them trapped grains of UO_x and then were transported to other premises of the reactor building, eventually mechanically detached from the substrate. Many of the crystals contain UO_x and $(\text{Zr}_{1-x}\text{U}_x)\text{O}_2$ inclusions. In several cases it is clear that external zones of zircon grew when the UO_x dendrites were already precipitated, as it follows from relative position of the inclusion and growth layers (Fig. 7C, D). The glass matrix composition of the black lava in the nearest zone around zircon crystals is slightly depleted in Zr and U content (Table 1). This might imply growth of (at least) the outer zones of the crystals during cooling of the lava flow.

An important and still unresolved question is temperature of “chernobylite” formation. Several approaches developed in mineralogy could be used to resolve this question and are based on investigation of morphology of zircon and trace elements composition. A peculiar feature of many $(\text{Zr}_{1-x}\text{U}_x)\text{SiO}_4$ crystals is dipyrmidal morphology, observed both in polished sections and on whole grains after partial dissolution of the lava fragments in acid (Anderson et al., 1993). Zircon morphology depends on several factors and direct application of classic mineralogical morphodrom (Pupin, 1980) would suggest very low temperatures of crystallization (550–600 °C), contradicting previous estimates of

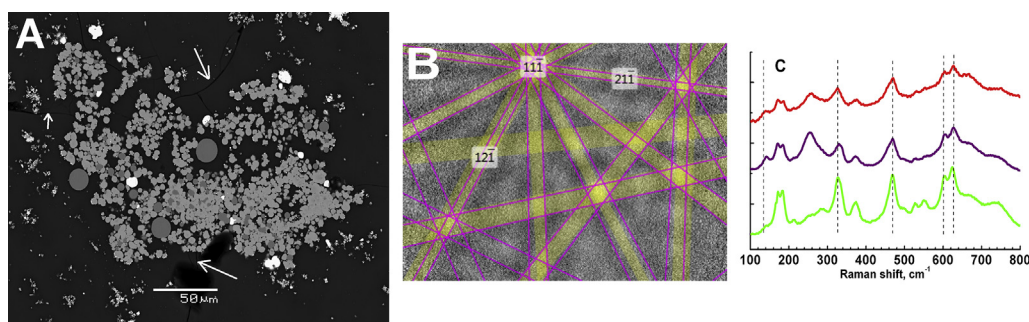


Fig. 6. A – BSE image of Zr-U-O phase in the brown lava. Bright spots – UO_2 , gray spheres – molten steel. Pronounced cracking, probably due to moisture-induced transition (see text), is indicated by arrows. B – EBSD pattern from the region in panel A. Kikuchi lines corresponding to tetragonal ZrO_2 (ICSD card #88022) are shown. C – Raman spectra of several points in panel A. Vertical dashed lines indicate positions of peaks of tetragonal ZrO_2 . Spectra are stacked up for clarity.

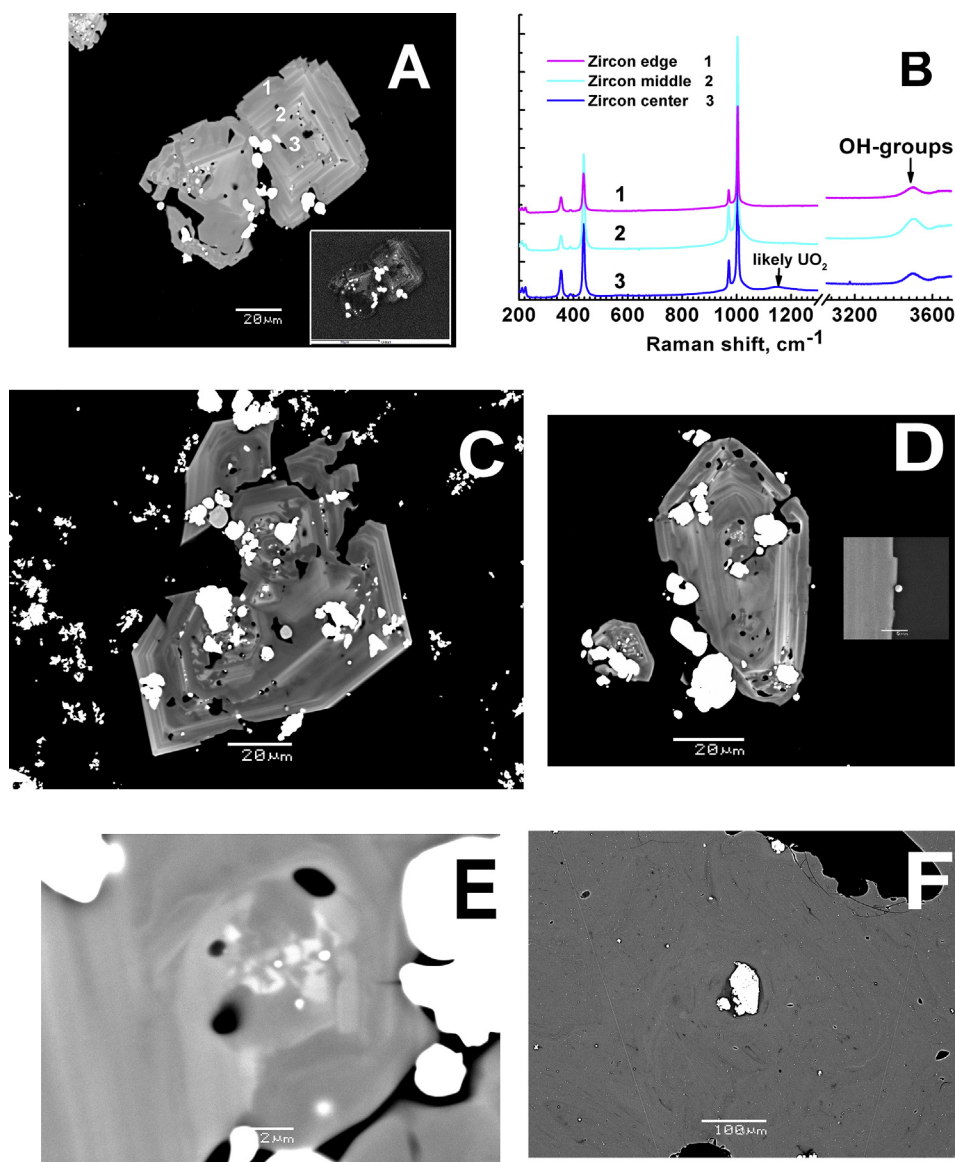


Fig. 7. Uranium-rich zircon – “Chernobylite”. A – BSE image of a zircon from Sample I; numbers show approximate location of spots for Raman spectroscopy. Inset shows EDX X-ray intensity map of the U $M\alpha$ line. B – Raman spectra from several growth zones of a zircon shown on panel A. Spectra are stacked up for clarity. C – BSE image of several intergrown skeletal zircon crystals with abundant urania inclusions. Note that some UO_2 dendrites cut zircons’ growth zones. D – relatively rare example of elongated zircon in sample II (BSE mode); the inset shows zoomed SE image of a steel ball at the right edge of the crystal. E – Growth center of a zircon crystal, SE mode. Small bright spots in the very center probably chemically differ from the zircon, though minute size precludes chemical analysis. F – BSE image of Sample II showing that at least some zircon crystals (same grain as in D) rotated during last stages of the lava solidification, indicating that they were formed at temperatures significantly higher than T_g of the lava.

“chernobylite” formation temperature. However, in-depth work by (Benisek and Finger, 1993) showed that high concentrations of uranium in growth medium strongly promote bipyramidal (i.e. {101}) morphology. Note also that artificial Pu- and Np-doped zircon crystals (Burakov et al., 2010) mostly possess the bipyramidal morphology, supporting the importance of the impurities for zircon shape.

Temperature of zircon decomposition into $ZrO_2 + SiO_2$ depends on grains size, impurities and other parameters and is close to 1670 °C (Butterman and Foster, 1967; Kaiser et al., 2008); this temperature limits maximal temperature of “chernobylite” formation. The lowest formation temperature is more difficult to constrain. As discussed above, the temperature of the lavas at their source should be at least 1450–1500 °C. The stainless steel droplets ($T_{melting} \sim 1450\text{--}1500$ °C) are never trapped as real inclusions (i.e. as inclusions intersecting zircon growth zones), but are present in

cavities and decorate surfaces of zircon crystals (Figs. 3 and 4 from Anderson et al. (1993), Fig. 7). Although inclusions entrapment is governed by many factors (e.g., wettability), the presence of the steel in the voids may indicate that these zircon crystals grew (or at least continued to grow) when steel has already solidified. Note that the lava flows in the steam-discharge corridor (i.e. several tens of meters from the lava source) were unable to melt steel tubes. This is not surprising, since above the glass transition temperatures (800–850 °C (Gonchar and Zhidkov, 2002)) viscous flow remains possible. Fig. 7F shows that before the lava solidification some of zircon crystals were already fully grown, since one can see traces of crystal rotation. Application of Ti in zircon thermometry (Pöml et al., 2013) suggests that “chernobylite” could grow around 1250 °C. However Ti concentration in the lava is lower than in geological samples used for calibration of this thermometer and, keeping in mind significant variations of Ti concentration in

“chernobylite” (Pöml et al., 2013) it is likely that this thermometer is not fully applicable to the lava. Significant deviations of the lava composition from geological materials, especially high enrichment in U and Zr, also makes impossible application zircon saturation thermometry (Hanchar and Watson, 2003).

Our examination of “chernobylite” inclusions shows that in all likelihood they grew at the expense of the Zr-U-O phase consumed to different extent (Fig. 5 in Anderson et al. (1993), Fig. 8). As noted above, the Zr-U-O phase contains both high- and low-temperature modifications of ZrO_2 , but admixture of uranium may noticeably change the phase diagram. Comprehensive studies (Butterman and Foster, 1967; Curtis and Sowman, 1953; Kaiser et al., 2008) showed that zircon forms from ZrO_2 and SiO_2 at temperatures between 1300 and 1600 °C and the rate of the synthesis increases rapidly between 1425 and 1535 °C. Similar increase of zircon nucleation rate around 1200 °C (Gokhale et al., 1969) was attributed to so-called Hedvall effect, namely, increased nucleation rate related to phase or polymorphic transformation in the substrate. Rearrangements of ZrO_n and SiO_4 complexes in zircon and displacive phase transition known to occur between 830 and 1150 °C (Mursic et al., 1992) could be responsible for changes in kinetics and rates of zircon formation in the lava. Since variations in uranium concentration in ZrO_2 influence the stability of its polymorphs, the “chernobylite” nucleation and growth probably occurred in relatively wide temperature range. Note presence of sub-micron inclusions in the growth center of one zircon crystal (Fig. 7E). Though their size prevents reliable chemical analysis, high contrast in BSE mode might suggest that these inclusions may chemically differ from zircon and be a uranium-rich phase. High-uranium zircon (chernobylite) was synthesized in few experiments only (Burakov et al., 2010; Journeau, 2006; possibly also Krasnorutskyy et al., 2012) and at present it is difficult to unambiguously assess kinetics and timescales of their formation.

3.3.4. Silicate dendrites

In the piece of the Sample III, mostly in the dark part, at least two generations of compositionally different silicate dendrites and sceptre crystals are observed (Fig. 9) (see also (Trotabas et al., 1993)). Though there is no obvious spatial correlation of these exolutions with other types of inclusions, they appear to be more abundant around contacts of the darker and brighter zones. Analysis of the dendrites chemistry is strongly influenced by surrounding glass matrix, but semi-quantitative estimation of a more abundant population (larger dendrites) gives a pyroxene with composition $(Ca_{0.08}Fe_{0.02}Cr_{0.02}Zr_{0.02})Al_{0.18}Mg_{1.86}Si_{1.82}O_{5.97}$. Note that presence of a diopside (a pyroxene variety) in the lava was

inferred from early XRD analysis (Borovoy et al., 1990). Dendrite formation is common in conditions of strong supercooling, during, for example, rapid quenching. Unfortunately, it is difficult to determine unambiguously the formation mechanism of the dendrites formation in the Sample III at the current stage. Phase diagram of iron-free pyroxene (e.g., Gasparik, 2014) suggests that formation of such dendrites in the absence of olivine ($(Mg, Fe)_2SiO_4$) implies that temperature of the melt exceeded 1550 °C and that the lava was quenched rapidly to avoid the olivine precipitation between 1400 and 1550 °C. These values are in agreement with other estimates of the lava temperatures. Devitrification processes often lead to formation of dendrites; at least some of urania inclusions in the lava were formed by this mechanism. Finally, dendrites may also form during prolonged reheating of a solidified material, which, in our case, can be caused by interaction of “old” and “new” lava portions. This scenario, however, looks the least plausible.

3.4. Aerosol particles

For general review of the aerosol behavior in the “Shelter” see (Ogorodnikov et al., 2008); modern data on aerosol behavior in the “Shelter” rooms relevant to the current study are described in Ogorodnikov et al. (2015). One of the most important results of these on-going studies is marked difference in amount of radioactive aerosols generated by different lava accumulations: whereas radioactivity of aerosols at higher levels of the “Shelter” collected at the major vent (so-called “Bypass”) is very low, radioactive particles are fairly abundant at the lower levels. Chemical and radionuclide composition of the particles collected with an air blower on the Petryanov filters, on the 1st floor of the Bubbler Tank (level 0.0 m), is consistent with origin from the lava accumulation described in Pazukhin et al. (2003). Dissolution of the filter in acetone or slow oxidation in air leaves numerous particles with variable morphology and composition. Quartz and various aluminosilicates are the main minerals (see also Borodin and Bryk, 2001; Kuzmina, 1997). Shapes of the glassy fragments indicate dispersion mechanism of their formation, but in many cases it is difficult to establish firmly their origin due to general abundance of concrete dust inside the “Shelter”.

The major fraction (~90%) of total activity of the filter pack (for results of nuclear spectroscopy and digital autoradiography see (Vlasova et al., 2015)) is retained on the frontal filter FPA-70-0.12, trapping particles $\geq 1 \mu m$. Some radioactive solid particles were able to penetrate two frontal filters and are retained by the last one (AFA RSP-20). The $^{137}Cs/^{241}Am$ ratio of the filter pack is lower

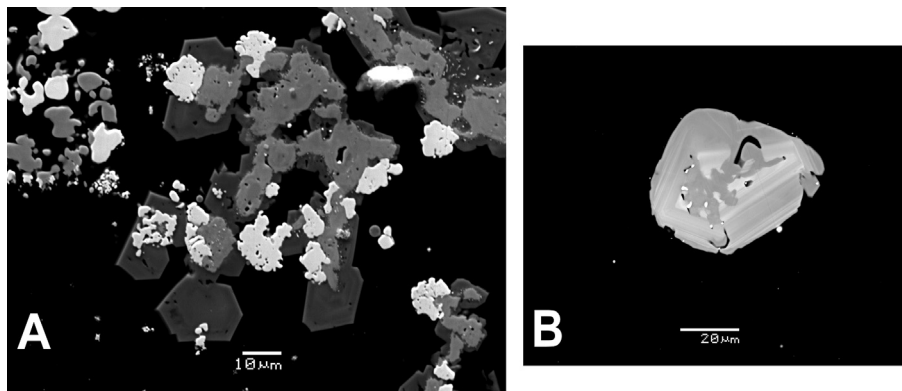


Fig. 8. Interaction between zircon and Zr-U-O phases. A – Zircon crystals overgrowing the Zr-U-O phase (SE mode). Bright spots – UO_2 precipitates; light gray – Zr-U-O phase; dark gray – U-rich zircon. B – Zonal zircon (BSE mode); the internal irregular zone reflects shape of consumed Zr-U-O nuclei. Small bright circles scattered in the matrix – steel droplets.

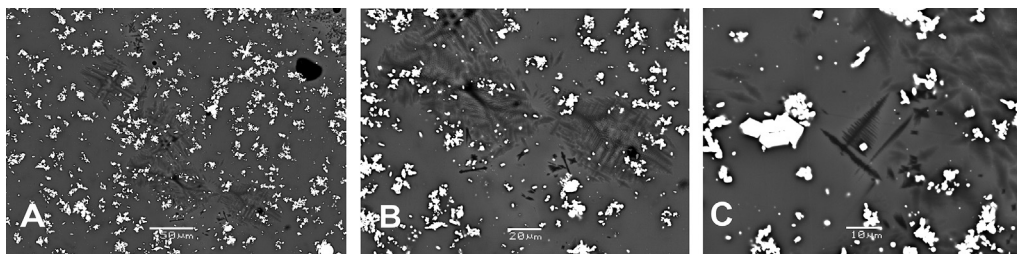


Fig. 9. Silicate dendrites with different morphologies in the sample of brown lava (sample III).

(12–19, see also (Ogorodnikov et al., 2013)) than that in “average” ChNPP fuel, indicating that the lava has lost part of volatile Cs. Parts of the filters containing “hot” spots on radiographic images were examined using X-ray tomography (Fig. 10D) which showed that in most cases the radioactivity is due to dense solid particles electrostatically attached to the filter threads (see also (Bogatov et al., 1990; Borodin and Bryk, 2001)). The weaker “hot” spots are at least partly associated with so-called condensation particles, formed by adsorption of Cs radioactive isotopes (and other nuclides) on dust and droplets (Bogatov et al., 1990; Kuzmina and Tokarevskii, 1997).

Track radiography and examination in BSE mode of the etched filters reveals spots with α -emitting nuclides. As expected, they are dominated by aggregates of U-rich particles (Fig. 10). In most cases the grains are isometric with sizes 200–400 nm and often form aggregates reaching 10–15 μm . These particles originate either from the lava accumulation or from pumice pieces possibly remaining in the room 012/7. Our results corroborate studies of ChNPP aerosols performed in mid-90ies where sub-micron U-rich particles attached to larger silicate or graphitic grains were observed (Kuzmina and Tokarevskii, 1997). Occasionally, urania particles up to approx. 10 μm are also observed (Fig. 10C). Absence of Zr and their morphology suggests that they most likely represent dispersed fuel dust.

3.5. Sub-mm individual particles from spontaneous lava decomposition

The radioactive particles were located in the collection filter using Imaging Plate. For results of nuclear spectroscopy and autoradiography see Vlasova et al. (2015). Individual particles reach $150 \times 200 \mu\text{m}$, most of them resembles chips of porous glass (pumice-like), see Fig. 11. Similar samples were obtained 11 years after the accident by taking smears from the lava in steam-discharge corridor (Kuzmina and Tokarevskii, 1997). The glass particles contain abundant U-rich inclusions with variable U/Zr ratio. Single-crystal X-ray diffraction indicates that the inclusions are represented by several intergrown single crystallites of UO_{2+x} ($x \sim 0.25$). This confirms earlier results that whereas urania dendrites in the lava bulk are very close to ideal stoichiometry (see above), in aerosols uranium is often more oxidized (e.g., Bogatov et al., 1990). Closer examination of the SEM images suggests dendrite-like shape of these inclusions, which is confirmed by X-ray tomography. Several Zr-containing particles with absent or very small α -radioactivity (Fig. 11E) were found. These particles may represent pieces of outer parts of zircaloy cladding which have not reacted with UO_2 .

Clusters of needle-like secondary crystals possibly represented by Na-uranyl-sulphates are frequently present on surfaces of the former bubbles. These mineral phases are weakly bound to the glass chips (Fig. 11C) and are presumably closely related to water-soluble uranium-containing secondary phases described in

Anderson et al. (1992b); Burakov et al. (1997b). SEM-EDX data on composition of different kinds of individual particles (pumice-like chips, non radioactive Zr-containing particles and secondary Na-U-S-O crystals) are presented in Table 3. Note that surface roughness of the particles makes the EDX analysis only semi-quantitative. Traces of aluminosilicates, P, Cl are present in spectra of the secondary uranyl minerals. The Zr impurity was observed only when the crystals reside on surfaces of the pumice-like fragments.

4. Discussion

Extensive efforts of numerous scientists provided detailed description of the process of explosion at Chernobyl NPP, its radiological and ecological consequences and gave a unique possibility to examine from material science point of view substances produced during interaction of hot nuclear fuel with concrete. The initial stages of the Chernobyl accident involving interaction of the fuel with zircaloy are broadly similar to Three-Mile (TMI) and Fukushima accidents and dedicated experiments. Temperatures of initiation of various steps of fuel-zircaloy reactions at ChNPP could be lower than in out-of-pile experiments due to non-negligible burn-up degree of ChNPP fuel (up to 13 GWd/tU (Arutyunyan et al., 2010),) (Bottomley et al., 1999).

Experiments and calculations simulating interaction of molten corium with concrete are invariably limited to relatively small masses of “corium” (tens of kilograms), whereas the Chernobyl accident has involved orders of magnitude larger masses with hugely bigger thermal inertia. Therefore, kinetics and timescales of the processes could have been very different and investigations of the products of the accident are extremely important. For example, investigation of drill cores from the lava and underlying concrete (Pazukhin, 2008; Dikiy et al., 2007) revealed significant actinides fractionation and showed importance of fluid metasomatism for the concrete alteration, the factors which are barely possible to address in laboratory-scale experiments. Important difference between the situation at ChNPP and experiments aimed at development of corium catcher (e.g., Gusarov et al., 2005; Journeau, 2006) is the composition of concrete: the catcher usually contains lots of Fe compounds, virtually absent in the Chernobyl concrete.

Very important difference between the Chernobyl and TMI accidents is the absence of corium-concrete interaction in the latter, leading to very different behavior of UO_2 , zircaloy, ZrO_2 and other compounds (Strain et al., 1989; Akers and McCardell, 1989; Hobbins et al., 1989). However, the accident at Fukushima NPP appears to be more relevant, since according to some models corium has interacted with the concrete (Tanabe, 2012) and with mineral wool from thermal insulation (Satou Y., in preparation). Indeed, U-containing glassy silicate hot particles with high concentration of Cs in external layers were collected in affected areas (Abe et al., 2014; Adachi et al., 2013). Presumably, material similar to the Chernobyl lava have also formed during the Fukushima accident, but is still not properly located.

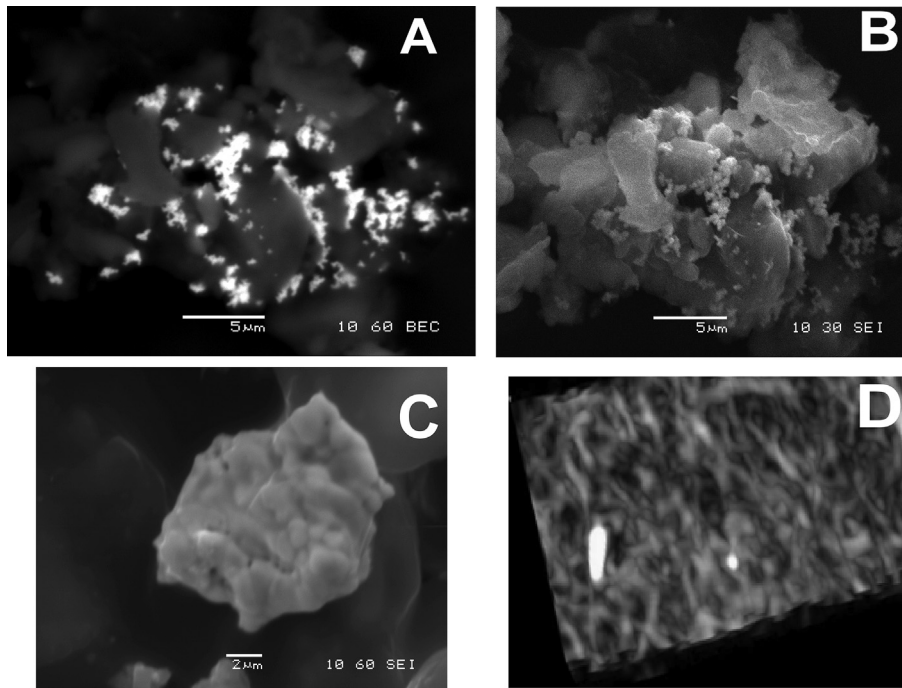


Fig. 10. Aerosol particles from filters. A, B – BSE and SE images of agglomeration of small particles with uranium. C – UO_{2+x} particle. D – image from X-ray tomography reconstruction of the aerosol filter with two hot particles (bright spots, confirmed by autoradiography). Field of view length – 2 mm.

Though international efforts to create a new, safer “Shelter” over the ChNPP are on advanced stage, the problem of handling thousands of tons of radioactive substances remains unsolved. Moreover, monitoring showed that ^{137}Cs activity in aerosols remained rather constant (with correction for decay) from July 1986 till 2005 (Ogorodnikov et al., 2006); α -contaminated dust is continuously produced by lava accumulations in room 304/3 of the “Shelter” (Badovskii et al., 2014). These facts clearly raise radiological concerns. Though qualitatively most of our findings corroborate earlier works, application of complementary experimental methods to aged (30 years old) lava-like fuel containing masses provided some interesting details, useful for assessment of their long-term behavior.

Natural lavas from Mt. Cameroon volcano in Africa may be used as a reference, although distant, to assess long-term stability of the Chernobyl lava. Basaltic lava flows from Mt. Cameroon are broadly similar to Chernobyl lava in silica content. The Cameroon volcano is unique in a sense that situated almost on equator and, being 4700 m high, it provides an opportunity to study alteration rate of silicate lavas in very broad range of humidity and temperature variations. It was shown (Chauvel et al., 2005) that even in unfavourable conditions, i.e. in the lower part of the mountain with very high precipitation rate, the thickness of the alteration crust does not exceed 10 cm in 100 years. However, tephra or pumice are altered at much higher rates (Dahlgren et al., 1999), presumably due to much higher surface area.

From the point of view of nuclear waste forms Chernobyl lava represents aluminosilicate glass-ceramics with abundant inclusions and pores. There is no doubt that destruction of the lava is an on-going process manifested in cracking of some of the lava flows and spontaneous destruction of individual lava samples in laboratory (Burakov, 2013b), aerosol formation by dispergation, detachment of larger particles and formation of secondary phases. However, the scale of the degradation phenomena is highly debatable. Several obvious mechanisms are important for the degradation: 1) self-irradiation; 2) thermomechanical cracking; 3)

leaching by water and interaction with atmospheric gases/vapours. Below we will consider these mechanisms based on literature data and our own results.

4.1. Influence of self-irradiation

The Chernobyl lava contain between 4 and 10 wt% of irradiated slightly enriched (2% of ^{235}U , (Arutyunyan et al., 2010),) nuclear fuel. The principal α -emitters are ^{235}U , Pu and Am isotopes. Fission products such as ^{137}Cs and ^{90}Sr determine β - and γ -contributions. Self-irradiation of a glass may lead to phase separation and defects formation, influencing leaching and mechanical stability. Dedicated experiments on radioactive dust generation by the lava in laboratory conditions (Baryakhtar et al., 2002) were interpreted as sub-micron dust formation due to sputtering of glass matrix by self-irradiation. Investigations of various types of nuclear glasses (e.g., Prokin et al., 1988; Weber et al., 1997) has shown that significant effects on glass performance are observed at cumulated doses exceeding $\sim 10^{18}$ α -decays/g and/or $\sim 10^9$ Gy. In case of Chernobyl lava in assumption of homogeneous distribution of α -emitters (for β - and γ -sources the homogeneity approximation always holds) such dose will be accumulated in $\sim 10^4$ years, which allowed to conclude (Pazukhin et al., 2002b) that self-irradiation is not a severe problem for this material. Our XAFS investigation of U local environment (this work) and spatial distribution of α -emitters and other radionuclides (Vlasova et al., 2015) favor hypothesis of even distribution of the activity on micron-scale level.

Despite pronounced radiation damage of acrylic resin holder during more than 20 years of storage, the studied samples preserved extremely smooth surface and sharp edges. The notable exception to this statement are the cracks surrounding large inclusions of UO_2 (Fig. 5A) and Zr-U-O phase (Fig. 6A). We have observed similar cracks in studies of Lanthanide borosilicate (LaBS) glasses doped with excessively high concentrations of Pu, which has led to precipitation of PuO_2 dendrites (Shiryayev et al., 2010; Stefanovsky et al., 2012). Cracking around those inclusions is

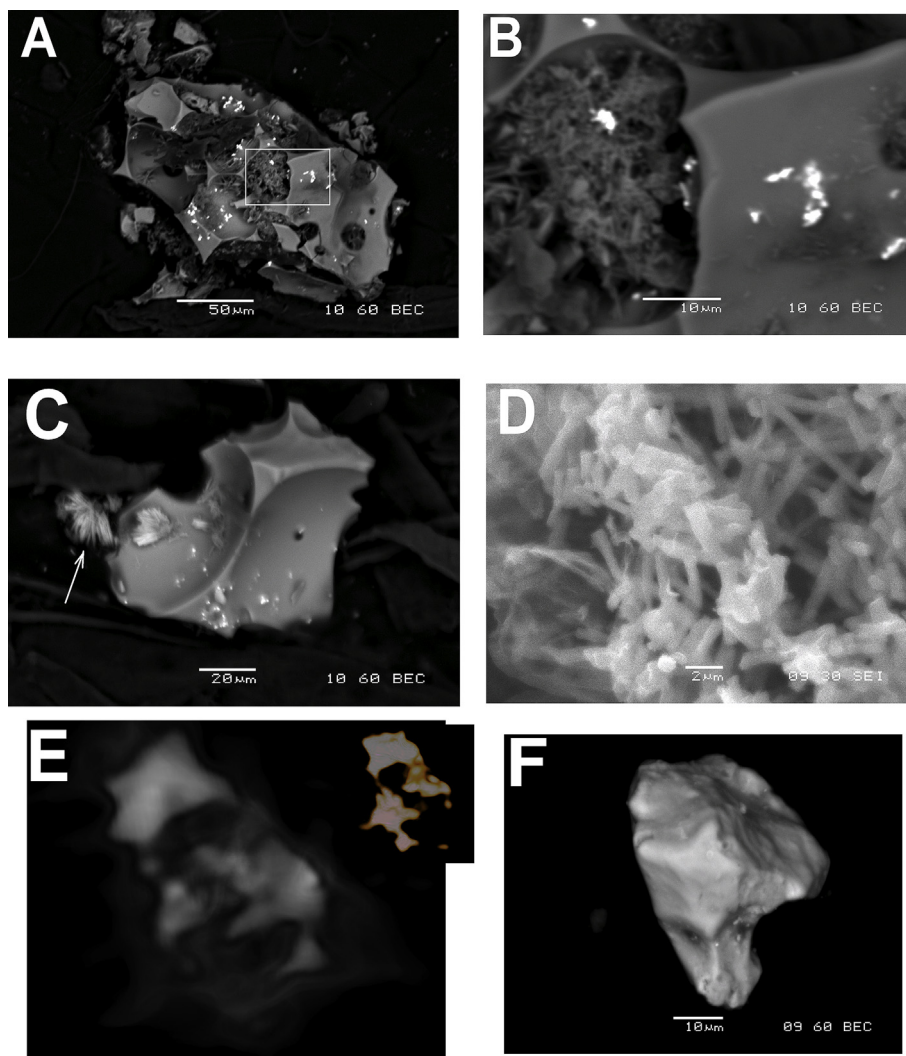


Fig. 11. SEM and X-ray images of spontaneously detached lava particles. A – general view of one of the particles; B – zoomed part of the A (marked by a rectangle) with visible secondary U-containing minerals and UO_{2+x} dendrites protruding from the particle's bulk. C – a particle with detached secondary minerals (indicated by an arrow). D – zoomed view of secondary alteration minerals. E – X-ray tomography reconstruction of the particle A, volume with higher density corresponding to UO_{2+x} dendrites is highlighted. F – BSE image of Zr non-radioactive particle.

Table 3

Composition^a (mass %) of individual U-containing particles that spontaneously detached from the lava flow from the Room 012/7; level 0.0 m. Number of measurements is in brackets. Literature data from Pazukhin (1994) are in *italic*.

Element	Pumice-like fragments		Zr particles (4)	<i>Bulk composition of pumice samples, BB-1</i>	<i>Bulk composition of slag samples, BB-1</i>
	Glass matrix (22)	Secondary U-containing crystals (9)			
Na	2.3 ± 0.8	30.2 ± 6.2		1.4 ± 0.2	1.5 ± 0.5
Mg	5.7 ± 0.5			4.6 ± 0.4	6.2 ± 2.2
Al	4.6 ± 0.3			2.8 ± 0.4	3.4 ± 1.4
Si	30.5 ± 0.8			36.6 ± 0.5	32.3 ± 2.3
S		13.1 ± 4.7			
K	1.7 ± 0.2		2.4 ± 1.6		
Ca	5.2 ± 0.6			4.5 ± 0.6	4.0 ± 1.1
Cr	0.3 ± 0.1				
Mn	0.4 ± 0.2				
Fe	0.7 ± 0.3			1.2 ± 0.3	0.8 ± 0.2
Zr	2.9 ± 0.3		60.2 ± 8.9	3.3 ± 0.5	4.5 ± 1.4
U	2.7 ± 0.5	6.1 ± 5.3	7.2 ± 5.1	8.3 ± 1	8.3 ± 0.2
O	43.6 ± 0.5	39.8 ± 2.5	25.2 ± 3.0		

^a - Semi-quantitative standardless SEM-EDX data.

obvious (Fig. 12), especially after leaching in hot water.

4.2. Mechanical degradation due to thermal stresses

Despite significant thermal inertia of the “Shelter” temperature variations may reach several tens degrees (depending on location in the building). Thermal cycling of the lava in laboratory (Gonchar and Zhidkov, 2001) demonstrated remarkable stability of the bulk material even in presence of the solid inclusions. Presumably, the only type of lava potentially prone to mechanical destruction is pumice-like and granulated material on the lower levels of the “Shelter” (both floors of the Bubbler). Note that lava accumulations on these levels contain 9 ± 3.5 tons of fuel (Arutyunyan et al., 2010). Indirect support of significantly lower aerosol-generating ability of these accumulations in comparison with bulk lava at upper levels comes from markedly lower radioactivity of aerosol filters from the latter locality (Khomutinin et al., 2012; Ogorodnikov et al., 2013).

4.3. Effect of water and chemical alteration

According to spectroscopic measurements reported here, the lava matrix is anhydrous. This is an important result, since water significantly influences properties of silicate glasses. Spatially-resolved study showed that OH-groups are detected only in relation to solid inclusions and/or possibly, in accompanying microcracks. Note that we have not observed H-O-H deformation band which would have indicate presence of molecular water in eventual pores. Experiments on leaching of radionuclides from the lava performed soon after the accident (Rogozin et al., 1991) and more recently (Krinityn et al., 1998) demonstrated that the leaching rate is comparable to nuclear glasses in relevant liquids.

However, interaction of the lava with water and atmospheric gases and vapors is not limited to simple leaching. Indeed as early as in 1990 formation of secondary uranium minerals was observed on surfaces of lava flows inside the “Shelter” (Anderson et al., 1992b; Burakov et al., 1997b). This process continues at present as shown in this paper (see paragraph 3.5). There is some indirect evidence that formation of chemically unstable uranyl minerals is possible even for lava sample stored under laboratory conditions (Burakov, 2013b).

In our view, the long-term stability of Chernobyl lava is determined by combination of the factors mentioned above. For the intrinsically fragile pumice-like and granular materials form the lower levels of the “Shelter” (thermo)mechanical degradation is likely prevailing. For the bulk material on the upper layers combination of moisture and self-radiation seem to be more important.

As mentioned above, moisture and self-irradiation may lead to significant volume expansion of ZrO_2 inclusions, leading to microcracking. Note that in most cases dispersed particles described here and by other researchers show signs of brittle fracturing. Formation of secondary uranium-rich mineralization on surfaces of the lava is another manifestation of water-induced degradation.

5. Conclusions

For the first time matrices of Chernobyl “lava” samples were studied by complementary methods such as vibrational spectroscopy (IR and Raman), X-ray Absorption Spectroscopy and tomography, electron microscopy and back-scattering electron diffraction. We have studied bulk samples stored in laboratory from 1991, aerosols and dispersed pieces of the lava collected in 2010–2014. It is shown that the matrix can be described as depolymerised met-aluminous silicate glass. The glass matrix is essentially anhydrous, but OH-groups are observed in zircon inclusions. Local devitrification of the glass matrix of the brown lava manifested in formation of pyroxene-like dendrites is observed. It is shown that the main fractions of U and Zr in the black lava reside in highly disordered atomic environment, i.e. in the glass matrix.

Raman spectroscopy shows that many of urania inclusions are characterized by very small deviations from the ideal UO_2 stoichiometry, Raman spectra of the Zr-U-O phase confirm that some of zirconia inclusions contain tetragonal ZrO_2 , most likely stabilized by uranium admixture. Transformation of the tetragonal to monoclinic zirconia modifications caused, for example, by moisture, provide an important, previously unrecognized mechanism of the lava destruction. Cracking is also observed around large inclusions of UO_2 .

Investigation of aerosols and of spontaneously detached lava particles showed that at least some lava accumulations in the “Shelter” building continue to degrade with formation of radioactive particles in the size range from <1 to $250 \mu m$. The pumice-like and granulated lava at the lowest levels of the building appear to be the most susceptible to thermomechanical destruction. Interaction of the lava with water or water vapor leads to formation of secondary water-soluble uranium-containing phases.

The principal factors affecting stability of the lava matrix are radiation damage from U-bearing inclusions (containing Am, Np and Pu as well) complemented by detrimental effect of water/moisture. For mechanically weak pieces of the lava, such as pumice, thermomechanical stresses play an important role. The degradation rate and related radiological danger remain uncertain.

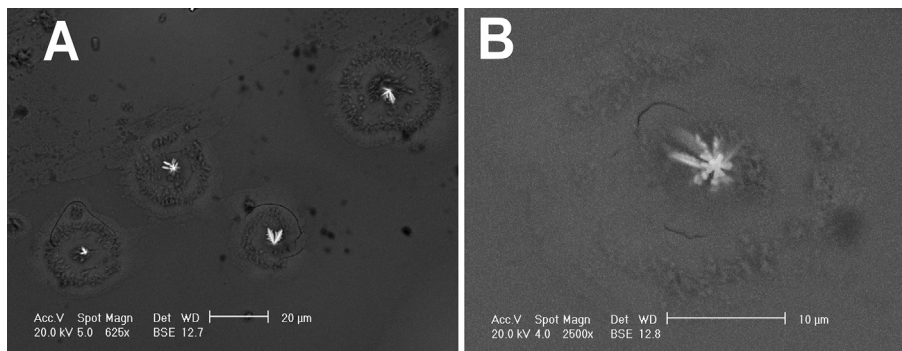


Fig. 12. BSE images of Lanthanide borosilicate glass doped with 9.5 wt% PuO_2 and subjected to 40 days of static leaching in $90^\circ C$ water after two years of storage at RT. Extensive cracking around precipitates of excess PuO_2 dendrites is clearly observed. A – general view; B – zoomed view of PuO_2 inclusion. Haloes around plutonia precipitates are due to clusters of radiation defects, revealed by the leaching.

Acknowledgements

The work was partly supported by RFBR grant N^o 03-16-00944 and IAEA CRP Contract No. 20546. Constructive comments of two anonymous reviewers are gratefully acknowledged.

References

- Abagyan, A.A., Arshavskii, I.M., Dmitriev, V.M., Kroshilin, A.E., Krayushkin, A.V., Khalimonchuk, V.A., 1991. Computational analysis of the initial stage of the accident at the Chernobyl atomic power plant. *Sov. At. Energy* 71 (4), 785–795.
- Abe, Y., Iizawa, Y., Terada, Y., Adachi, K., Igarashi, Y., Nakai, I., 2014. Detection of uranium and chemical state analysis of individual radioactive microparticles emitted from the Fukushima nuclear accident using multiple synchrotron radiation X-ray analyses. *Anal. Chem.* 86, 8521–8525.
- Adachi, K., Kajino, M., Zaizen, Y., Igarashi, Y., 2013. Emission of spherical caesium-bearing particles from an early stage of the Fukushima nuclear accident. *Sci. Rep.* 3, 2554 (5 pp).
- Adamov, E.O., Vasilevskii, V.P., Ionov, A.I., Nikitin, Yu.M., Panin, V.M., Podlazov, L.N., Stenbok, I.A., Rogova, V.D., Cherkashov, Yu.M., 1988. Analysis of the first phase of the development of the accident in the fourth block of the Chernobyl Atomic Power Station. *Sov. At. Energy* 64 (1), 27–33.
- Akers, D.W., McCardell, R.K., 1989. Core materials inventory and behavior. *Nucl. Technol.* 87, 214–223.
- Anderson, E.B., Burakov, B.E., Pazukhin, E.M., 1992a. Some peculiarities of chemical composition and morphology of fuel particles from near zone of Chernobyl NPP. *Radiochemistry* 34 (5), 139–144.
- Anderson, E.B., Burakov, B.E., Pazukhin, E.M., 1992b. Secondary alterations of fuel-containing masses of 4th unit of Chernobyl NPP. *Radiochemistry* 34 (5), 135–138.
- Anderson, E.B., Burakov, B.E., Pazukhin, E.M., 1993. High-uranium zircon from “Chernobyl lavas”. *Radiochim. Acta* 60, 149–151.
- Arutyunyan, R.V., Bolshov, L.A., Borovoi, A.A., Velikhov, E.P., Klyuchnikov, A.A., 2010. Nuclear Fuel in the «Shelter» Encasement of the Chernobyl NPP. *Nauka, Moscow*, p. 240.
- Badovskii, V.P., Melenevskii, A.E., Morozov, Yu.V., Ushakov, I.A., Shcherbin, V.N., 2014. Generation of radioactive dust by lava-like fuel-containing materials at the shelter object of Chernobyl NPP. *Radiochemistry* 56 (3), 311–318.
- Baryakhtar, V., Gonchar, V., Zhidkov, A., Zhydkov, V., 2002. Radiation damages and self-sputtering of high-radioactive dielectrics: spontaneous emission of sub-micronic dust particles. *Condens. Matter Phys.* 5 (3), 449–471.
- Benisek, A., Finger, F., 1993. Factors controlling the development of prism faces in granite zircons: a microprobe study. *Contrib. Mineral. Pet.* 114, 441–451.
- Bogatov, S.A., Borovoi, A.A., Dubasov, Yu.V., Lomonosov, V.V., 1990. Form and parameters of the particles of the fuel ejection in the Chernobyl reactor accident. *Sov. At. Energy* 69 (1), 595–601.
- Borodin, O.V., Bryk, V.V., 2001. Investigation of particles extracted by dust-retaining films and smears from the “Shelter” object. *Problems Atomic Sci. Technol.* 80, 72–75.
- Borovoi, A.A., Galkin, B.Ya., Drapchinskii, L.V., Krinitsyn, A.P., Pazukhin, E.M., Petrov, B.F., Pleskachevskii, L.A., Checherov, K.P., 1991a. Artificial products of interaction of fuel with construction materials of 4th unit of Chernobyl NPP. III. Bubbler basin – radiation situation and fuel-containing masses. *Sov. Radiochem.* 33 (4), 177–196.
- Borovoi, A.A., Galkin, B.Ya., Krinitsyn, A.P., Pazukhin, E.M., Kheruvimov, A.N., Checherov, K.P., Anderson, E.B., 1991b. Artificial products of interaction of fuel with construction materials of 4th unit of Chernobyl NPP. IV. Steam distribution collector and some drill core materials. *Sov. Radiochem.* 33 (4), 197–210.
- Borovoi, A.A., Lagunenka, A.S., Pazukhin, E.M., 1998. Estimating the amount of fuel in cellar building 305/2 at Chernobyl unit 4. *At. Energy* 84 (4), 295–299.
- Borovoi, A.A., Lagunenka, A.S., Pazukhin, E.M., 1999. Radiochemical and some physico-chemical features of samples of lava and of concrete from sub-reactor room 304/3 of 4th unit of ChAES. Their relation with scenario of the accident. *Radiochemistry* 41 (2), 197–202.
- Borovoy, A.A., Galkin, B.Ya., Krinitsyn, A.P., Markushev, V.M., Pazukhin, E.M., Kheruvimov, A.N., Checherov, K.P., 1990. Artificial products of interaction of fuel with construction materials of 4th unit of Chernobyl NPP. *Sov. Radiochem.* 32, 103–113.
- Bottomley, P.D., Coquerelle, M., 1989. Metallurgical examination of bore samples from the Three Mile Island unit 2 reactor core. *Nucl. Technol.* 87 (1), 120–136.
- Bottomley, P.D.W., Glatz, J.-P., Barrachin, M., 1999. Irradiated UO₂ fuel dissolution by molten Zircaloy: results from SCA Corium interaction thermochemistry project. In: *Proceedings of the Workshop Severe Accident Research in Japan '99 (SARJ '99)*, pp. 123–129.
- Brown, A., McIntyre, G.J., Graslund, C., 1989. Analysis of crystalline phases in core bore materials from Three Mile Island unit 2. *Nucl. Technol.* 87 (1), 137–145.
- Burakov, B.E., 2013a. Crystalline Mineral-like Forms for Actinides Immobilization. Habilitation thesis. Sankt-Petersburg University.
- Burakov, B.E., 2013b. Material study of Chernobyl “lava” and “hot” particles. In: *International Experts' Meeting on Decommissioning and Remediation after a Nuclear Accident*. <http://www-pub.iaea.org/iaea meetings/IEM4/30Jan/Burakov.pdf>.
- Burakov, B.E., Anderson, E.B., Galkin, B.Ya., Pazukhin, E.M., Shabalev, S.I., 1994. Study of Chernobyl “hot” particles and fuel containing masses: implications for reconstruction the initial phase of the accident. *Radiochim. Acta* 65, 199–202.
- Burakov, B.E., Anderson, E.B., Shabalev, S.I., Strykanova, E.E., Ushakov, S.V., Trotabas, M., Blanc, J.-Y., Winter, P., Duco, J., 1997a. The behavior of nuclear fuel in first days of the Chernobyl accident. In: Gray, W.J., Triay, I.R. (Eds.), *Scientific Basis for Nuclear Waste Management XX*, Mat. Res. Soc. Symp. Proc. 465, Warrendale, PA, vol. 465, pp. 1297–1308.
- Burakov, B.E., Anderson, E.B., Strykanov, E.E., 1997b. Secondary uranium minerals on the surface of Chernobyl “lava”. In: *Materials Research Society Symposium Proceedings Scientific Basis for Nuclear Waste Management XX*, vol. 465, pp. 1309–1311.
- Burakov, B.E., Shabalev, S.I., Anderson, E.B., 2003. Principal features of chernobyl hot particles: phase, chemical and radionuclide compositions. In: Barany, S. (Ed.), *Role of Interfaces in Environmental Protection*, NATO Science Series, Earth and Environmental Sciences, 24. Kluwer Academic Publishers, pp. 145–151.
- Burakov, B.E., Ojovan, M.I., Lee, W.E., 2010. Crystalline Materials for Actinide Immobilisation. In: *Materials for Engineering*, vol. 1. Imperial College Press, London, p. 197.
- Butterman, W.C., Foster, W.R., 1967. Zircon stability and the ZrO₂–SiO₂ phase diagram. *Am. Mineral.* 52, 880–885.
- Chauvel, C., Dia, A.N., Bulourde, M., Chabaux, F., Durand, S., Ildefonso, P., Gerard, M., Deruelle, B., Ngounouno, I., 2005. Do decades of tropical rainfall affect the chemical compositions of basaltic lava flows in Mount Cameroon? *J. Volcanol. Geotherm. Res.* 141, 195–223.
- Chernyshov, A.A., Veligzhanin, A.A., Zubavichus, Y.V., 2009. Structural materials science end-station at the Kurchatov synchrotron radiation source: recent instrumentation upgrades and experimental results. *Nucl. Instrum. Methods Phys. Res. A* 603, 95–98.
- Chevalier, J., Gremillard, L., 2009. The tetragonal-monoclinic transformation in zirconia: lessons learned and future trends. *J. Am. Ceram. Soc.* 92 (9), 1901–1920.
- Corrections. *Geostand. Newsl.* 4 (1), 1980, 257–258.
- Curtis, C.E., Sowman, H.G., 1953. Investigation of the thermal dissociation, reassociation and synthesis of zircon. *J. Am. Ceram. Soc.* 36, 190–198.
- Dahlgren, R.A., Ugolini, F.C., Casey, W.H., 1999. Field weathering rates of Mt. St. Helens tephra. *Geochim. Cosmochim. Acta* 63 (5), 587–598.
- Dikiy, N.P., Dedik, A.N., Dovbnya, A.N., Uvarov, V.L., Shevyakova, E.P., 2007. Features of high-temperature diffusion in concrete at the 4th block of the Chernobyl NPP. *Radiochemistry* 49 (4), 426–431.
- Farges, F., Rossano, S., 2000. Water in Zr-bearing synthetic and natural glasses. *Eur. J. Miner.* 12 (6), 1093–1107.
- Gasparik, T., 2014. *Phase Diagrams for Geoscientists*. Springer-Verlag, New York, p. 462.
- Geisler, T., Burakov, B.E., Zirlin, V., Nikolaeva, L., Poml, P., 2005. A Raman spectroscopic study of high-uranium zircon from the Chernobyl “lava”. *Eur. J. Mineral.* 17, 883–894.
- Gokhale, K.V.G.K., Ramani, S.V., Subarrao, E.C., 1969. Hedvall effect and synthesis of zircon. *J. Mater. Sci.* 4, 468–469.
- Gonchar, V.V., Zhidkov, A.V., 2001. Behaviour of lava-like fuel-containing materials of the object “Shelter” during thermal treatment. *Problems Nucl. Power Plants Saf. Chernobyl* 8, 53–58.
- Gonchar, V.V., Zhidkov, A.V., 2002. Dynamics of high-temperature interaction of damaged nuclear fuel with construction materials of RBMK. *Problems Nucl. Power Plants Saf. Chernobyl* 9, 25–33.
- Graves, P.R., 1990. Raman microprobe spectroscopy of uranium dioxide single crystals and ion implanted polycrystals. *Appl. Spectrosc.* 44 (10), 1665–1667.
- Gusarov, V.V., Almjashv, V.I., Khabensky, V.B., Beshta, S.V., Granovsky, V.S., 2005. Physicochemical modeling and analysis of the interaction between a core melt of the nuclear reactor and a sacrificial material. *Glass Phys. Chem.* 31 (1), 53–66.
- Hanchar, J.M., Watson, E.B., 2003. Zircon saturation thermometry. *Rev. Mineral. Geochem.* 53, 89–112.
- Hobbins, R.R., Russell, M.L., Olsen, C.S., McCardell, R.K., 1989. Molten material behavior in the Three Mile island unit 2 accident. *Nucl. Technol.* 87, 1005–1012.
- Hofmann, P., Hagen, S.J.L., Schanz, G., Skokan, A., 1989. Reactor core materials interactions at very high temperatures. *Nucl. Technol.* 87 (1), 146–186.
- Information on the accident at the Chernobyl nuclear power plant and its consequences prepared for IAEA. *Sov. At. Energy* 61 (5), 1986, 845–868.
- Journeau, C., 2006. L'etalement du corium: hydrodynamique, rhéologie et solidification d'un bain d'oxydes a hautes temperatures. PhD thesis. Université d'Orleans.
- Kaiser, A., Lobert, M., Telle, R., 2008. Thermal stability of zircon (ZrSiO₄). *J. Eur. Ceram. Soc.* 28, 2199–2211.
- Kashparov, V.A., Ivanov, Yu.A., Khomutinin, Yu.V., Pazukhin, E.M., 1996. An estimate of effective temperature and annealing duration of fuel particles ejected from Chernobyl reactor during the accident. *Radiochemistry* 38 (1), 84–89.
- Kashparov, V.A., Ivanov, Yu.A., Protsak, V.M., Khomutinin, Yu.V., Yoshchenko, V.I., Pazukhin, E.M., 1997. An estimate of maximal effective temperature and of duration of non-isothermal annealing of Chernobyl fuel particles during the accident. *Radiochemistry* 39 (1), 63–67.
- Khomutinin, Y.V., Protsak, V.P., Khan, V.Y., Ogorodnikov, B.I., 2012. Monitoring of release of radioactive aerosols from the object “Shelter” in 2011. *Problems Nucl. Power Plants Saf. Chernobyl* 19, 94–103.
- Kim, B.-K., Hamaguchi, H., 1997. Mode assignments of the Raman spectrum of monoclinic zirconia by isotopic exchange technique. *Phys. Status Solidi (B)* 203

- (2), 557–563.
- Kim, D.-J., Jung, H.-J., Yang, I.-S., 1993. Raman spectroscopy of tetragonal zirconia solid solution. *J. Am. Chem. Soc.* 76 (8), 2106–2108.
- Kiselev, A.N., Checherov, K.P., 2001. Model of the destruction of the reactor in the No. 4 unit of the Chernobyl nuclear power plant. *At. Energy* 91 (6), 967–975.
- Krasnorutskyy, V.S., Yakovlev, V.K., Danilov, A.P., Evseev, V.M., Matyuschenko, R.V., Kushnym, Ya.A., 2010. Microstructural analysis of lava-like fuel containing masses. *Problems Atomic Sci. Technol.* 95, 60–67.
- Krasnorutskyy, V.S., Yakovlev, V.K., Danilov, A.P., Slabospitskaya, E.A., Evseev, V.M., Matyuschenko, R.V., Tolstolutsky, A.G., 2012. Investigation of interaction of nuclear fuel with construction materials of the core in case of severe accident. *Problems Atomic Sci. Technol.* 78, 56–67.
- Krinityn, A.P., Simanovskaya, I.Ya., Strikhar, O.L., 1998. Investigation of interaction of water with construction and fuel-containing materials in premises of the “Shelter”. *Radiochemistry* 40 (3), 287–297.
- Kuzmina, I.E., 1997. Nuclear fuel and the characteristics of aerosol formation in the object “Cover”. *At. Energy* 82 (1), 38–43.
- Kuzmina, I.E., Tokarevskii, V.V., 1997. Sources and mechanisms of aerosol formation in the Chernobyl “Sarcophagus”. *At. Energy* 82 (2), 129–135.
- Lebedev, I.A., Myasoedov, B.F., Pavlotskaya, F.I., 1992. Frenkel V.Ya., Plutonium content in soils of the European part of the country after the accident at Chernobyl nuclear generating station. *At. Energy* 72 (6), 515–520.
- Manara, D., Renker, B., 2003. Raman spectra of stoichiometric and hyperstoichiometric uranium dioxide. *J. Nucl. Mater.* 321, 233–237.
- McMillan, P., 1984. Structural studies of silicate glasses and melts—applications and limitations of Raman spectroscopy. *Am. Mineralogist* 69, 622–644.
- Mursic, Z., Vogt, T., Frey, F., 1992. High-temperature neutron powder diffraction study of $ZrSiO_4$ up to 1900 K. *Acta Cryst.* B48, 584–590.
- Mysen, B.O., Toplis, M.J., 2007. Structural behavior of Al^{3+} in peralkaline, metaluminous, and peraluminous silicate melts and glasses at ambient pressure. *Am. Mineralogist* 92 (5–6), 933–946.
- Ogorodnikov, B.I., Budyka, A.K., Pazukhin, E.M., Krasnov, V.A., 2006. Aerosol emissions from the destroyed power-generating unit of the Chernobyl nuclear power plant in 1986 and 2003–2005. *At. Energy* 100 (4), 264–270.
- Ogorodnikov, B.I., Pazuhin, E.M., Klyuchnikov, A.A., 2008. Radioactive Aerosols of the “Shelter” Object 1986–2006. Institute for Safety Problems of NPP NASU, p. 456.
- Ogorodnikov, B.I., Khan, V.E., Kovalchuk, V.P., 2013. Aerosols as witnesses of destruction of lava-like fuel containing materials in the object “UKRITTYA”. *Problems Nucl. Power Plants Saf. Chernobyl* 20, 94–106.
- Ogorodnikov, B.I., Budyka, A.K., Khan, V.E., 2015. Specific features of radioactive aerosols in subreactor rooms of the shelter object of Chernobyl NPP. *Radiochemistry* 57 (6), 652–660.
- Pazukhin, E.M., 1994. Lava-like fuel-containing masses of 4th unit of Chernobyl NPP: topography, physical-chemical properties, scenario of formation. *Radiochemistry* 36 (2), 97–142.
- Pazukhin, E.M., 2008. Interaction of lava-like fuel-containing masses with structural concrete in the active phase of the Chernobyl accident. *Radiochemistry* 50 (3), 324–331.
- Pazukhin, E.M., Borovoi, A.A., Lagunenka, A.S., Kolomiets, F.N., 2002a. Investigation of LFCM materials sampled from different depths in lava flows. *Problems Nucl. Power Plants Saf. Chernobyl* 9, 66–75.
- Pazukhin, E.M., Borovoi, A.A., Rudya, K.G., 2002b. Effect of α -ray self-irradiation on stability of lava-like fuel-containing masses from the fourth block of the Chernobyl NPP. *Radiochemistry* 44 (6), 558–563.
- Pazukhin, E.M., Borovoi, A.A., Klyuchnikov, A.A., Krasnov, V.A., Lagunenka, A.S., Gavrilov, S.L., 2003. Bubbler basin and steam-distribution corridor of the Chernobyl NPP Block 4: new data. *Radiochemistry* 45 (2), 201–208.
- Pazukhin, E.M., Lagunenka, A.S., Krasnov, V.A., Bil'ko, V.V., 2006. Fuel at upper levels of the destroyed fourth block of Chernobyl NPP. refining the formation scenario of the polychromatic ceramics. *Radiochemistry* 48 (5), 522–534.
- Pöml, P., Burakov, B., Geisler, T., Walker, C.T., Grange, M.L., Nemchin, A.A., Berndt, J., Fonseca, R.O.C., Bottomley, P.D.W., Hasnaoui, R., 2013. Micro-analytical uranium isotope and chemical investigations of zircon crystals from the Chernobyl “lava” and their nuclear fuel inclusions. *J. Nucl. Mater.* 439, 51–56.
- Prokin, E.S., Kuptsov, V.S., Anakina, T.N., Ermolaev, E.E., 1988. Characterisation of borosilicate glass at modeling of alpha-radiation and thermal conditions of storage of highly active vitrified waste. *Sov. Radiochem.* 32 (5), 694–698.
- Pupin, J.P., 1980. Zircon and granite petrology. *Contrib. Min. Pet.* 73, 207–220.
- Rogozin, Yu.M., Smirnova, E.A., Savonenkov, V.G., Krivokhatsky, A.S., Avdeev, V.A., Sagaidachenko, E.Yu., 1991. Leaching of radionuclides from some newly formed products, extracted from reactor zone of 4th unit of Chernobyl NPP. *Radiochemistry* 33 (4), 160–167.
- Savonenkov, V.G., Krivokhatskii, A.S., Dubasov, Yu.V., Pazukhin, E.M., 1991. Radioactive man-made formations from the destroyed 4th Unit of Chernobyl NPP. *Sov. Radiochem.* 33 (4), 140–149.
- Shalaya, E.V., Murzakaev, A.M., Makarov, V.V., Pushin, V.G., Zamyatin, D.A., Shchapova, Yu.V., Votyakov, S.L., 2015. Localization of uranium in radiation-damaged nanoheterogeneous natural zircon. *Glass Phys. Chem.* 41 (4), 389–397.
- Shiryayev, A.A., Zubavichus, Ya.V., Stefanovsky, S.V., Ptashkin, A.G., Marra, J.C., 2010. EXAFS of Pu and Hf LIII edge in lanthanide-borosilicate glass. In: Burakov, B.E., Aloy, A.S. (Eds.), *Scientific Basis for Nuclear Waste Management XXXIII*, Mater. Res. Soc. Symp. Proc. 1193, Sankt-Petersburg, Russia, pp. 259–265.
- Stefanovsky, S.V., Shiryayev, A.A., Zubavichus, J.V., Veligjanin, A.A., Marra, J.C., 2009. Valence state and structure position of uranium ions in borosilicate glasses with high iron and aluminium contents. *Glass Phys. Chem.* 35 (2), 141.
- Stefanovsky, S.V., Shiryayev, A.A., Vlasova, I.E., Yapaskurt, V.O., Marra, J.C., 2012. Electron microscopy and Raman spectroscopy study of Pu-bearing LaBS glasses. In: *Actinides and Nuclear Energy Materials*. Mater. Res. Soc. Symp. Proc., vol. 1444. <http://dx.doi.org/10.1557/opl.2012.950>.
- Strain, R.V., Neimark, L.A., Sanecki, J.E., 1989. Fuel relocation mechanisms based on microstructures of debris. *Nucl. Technol.* 87, 187–190.
- Sweet, J.R., White, W.B., 1969. Study of sodium silicate glasses and liquids by infrared spectroscopy. *Phys. Chem. Glas.* 10, 246–251.
- Tanabe, F., 2012. Analyses of core melt and re-melt in the Fukushima Daiichi nuclear reactors. *J. Nucl. Sci. Technol.* 49 (1), 18–36.
- Teterin, Yu.A., Baev, A.S., Bogatov, S.A., 1994. X-Ray photoelectron study of samples containing reactor fuel from “lava” and products growing on it which formed at Chernobyl NPP due to the accident. *J. Electron Spectrosc. Relat. Phenom.* 68, 685–694.
- Trotabas, M., Blanc, J.-Y., Burakov, B., Anderson, E., Duco, J., 1993. Examination of Chernobyl Samples Impact on the Accident Scenario Understanding. Report DMT/92/309, SETIC/LECR-92/36; Report IPSN/93/02; Report RI-1-63/92.
- Ushakov, S.V., Burakov, B.E., Shabalev, S.I., Anderson, E.B., 1997. Interaction of UO_2 and zircaloy during the Chernobyl accident. In: *Materials Research Society Symposium Proceedings Scientific Basis for Nuclear Waste Management XX*, vol. 465, pp. 1313–1318.
- Vlasova, I., Shiryayev, A., Ogorodnikov, B., Burakov, B., Dolgoplova, E., Senin, R., Averin, A., Zubavichus, Y., Kalmykov, S., 2015. Radioactivity distribution in fuel-containing materials (Chernobyl “lava”) and aerosols from the Chernobyl “Shelter”. *Radiat. Meas.* 83, 20–25.
- Voronov, N.M., Voitekhova, E.A., Danilin, A.S., 1958. Phase equilibrium diagrams of the UO_2 - ZrO_2 and ThO_2 - ZrO_2 systems. In: *Proc. 2nd U.N. Intern. Conf. Peaceful Uses At. Energy*, Geneva, vol. 6, pp. 221–225.
- Weber, W.J., Ewing, R.C., Angell, C.A., Arnold, G.W., Cormack, A.N., Delaye, J.M., Grisco, D.L., Hobbs, L.W., Navrotsky, A., Price, D.L., Stoneham, A.M., Weinberg, M.C., 1997. Radiation effects in glasses used for immobilization of high-level waste and plutonium disposition. *J. Mater. Res.* 12 (8), 1948–1978.
- Wolten, G.M., 1958. Solid-phase transitions in the UO_2 - ZrO_2 system. *J. Am. Chem. Soc.* 80 (18), 4772–4775.
- Zamyatin, D.A., Shchapova, Yu.V., Votyakov, S.L., Eremin, N.N., Urusov, V.S., 2013. Structure and thermodynamic properties of zircon-coffinite solid solutions according to the semiempirical atomistic simulation data. *Glass Phys. Chem.* 39 (2), 182–192.
- Zhidkov, A.V., Gonchar, V.V., Veklich, E.L., Maslov, D.M., Pazukhin, E.M., Parkhomchuk, P.E., Chemersky, G.F., 2000. Some aspects of interaction of surfaces of various types of fuel-containing materials of the “Shelter” with water. *Problems Nucl. Power Plants Saf. Chernobyl* 6, 220–224.